Available online at www.sciencedirect.com
ScienceDirect
Solar Energy 85 (2011) 1580–1608
SOLAR ENERGY
www.elsevier.com/locate/solener

Solar photovoltaic electricity: Current status and future prospects

T.M. Razykov [a,b,c,*], C.S. Ferekides [b], D. Morel [b], E. Stefanakos [b], H.S. Ullal [d], H.M. Upadhyaya [e]

[a] Physical–Technical Institute, Scientific Association "Physics-Sun", Uzbek Academy of Sciences, G. Mavlyanov Street 2B, Tashkent 700084, Uzbekistan
[b] Department of Electrical Engineering, University of South Florida, 4202 E. Fowler Ave., ENB 0118 Tampa, FL 33620-5350, USA
[c] 43600 Solar Energy Research Institute, UKM, Bangi, Selangor, Malaysia
[d] National Center for Photovoltaics, National Renewable Energy Laboratory, Golden, CO 80401, USA
[e] CREST, Loughborough University, Leicestershire LE11 3TU, UK

Available online 3 January 2011

Communicated by: Associate Editor Yogi Goswami

Abstract

We review the technical progress made in the past several years in the area of mono- and polycrystalline thin-film photovoltaic (PV) technologies based on Si, III–V, II–VI, and I–III–VI_2 semiconductors, as well as nano-PV. PV electricity is one of the best options for sustainable future energy requirements of the world. At present, the PV market is growing rapidly at an annual rate of 35–40%, with PV production around 10.66 GW in 2009. Si and GaAs monocrystalline solar cell efficiencies are very close to the theoretically predicted maximum values. Mono- and polycrystalline wafer Si solar cells remain the predominant PV technology with module production cost around $1.50 per peak watt. Thin-film PV was developed as a means of substantially reducing the cost of solar cells. Remarkable progress has been achieved in this field in recent years. CdTe and $Cu(In,Ga)Se_2$ thin-film solar cells demonstrated record efficiencies of 16.5% and almost 20%, respectively. These values are the highest achieved for thin-film solar cells. Production cost of CdTe thin-film modules is presently around $0.76 per peak watt.

Keywords: Solar; Photovoltaics; Wafer; Thin film; Photovoltaic market; Nanophotovoltaics

1. Introduction

Presently, the world energy consumption is 10 terawatts (TW) per year, and by 2050, it is projected to be about 30 TW. The world will need about 20 TW of non-CO_2 energy to stabilize CO_2 in the atmosphere by mid-century. The simplest scenario to stabilize CO_2 by mid-century is one in which photovoltaics (PV) and other renewables are used for electricity (10 TW), hydrogen for transportation (10 TW), and fossil fuels for residential and industrial heating (10 TW) (Zweibel, 2005). Thus, PV will play a significant role in meeting the world future energy demand. The present is considered as the "tipping point" for PV (Kazmerski, 2006).

The PV effect was discovered in 1839 by Becquerel while studying the effect of light on electrolytic cells. A long period was required to reach sufficiently high efficiency. Solar cells developed rapidly in the 1950s owing to space programs and used on satellites (crystalline Si, or c-Si, solar cells with efficiency of 6–10%). The energy crisis of the 1970s greatly stimulated research and development (R&D) for PV.

Solar cells based on compound semiconductors (III–V and II–VI) were first investigated in the 1960s. At the same time, polycrystalline Si (pc-Si) and thin-film solar cell technologies were developed to provide high production capacity at reduced material consumption and energy input in the fabrication process, and integration in the structure

* Corresponding author at: Physical–Technical Institute, Scientific Association "Physics-Sun", Uzbek Academy of Sciences, G. Mavlyanov Street 2B, Tashkent 700084, Uzbekistan. Tel.: +998 71 135 4103; fax: +998 71 135 4291.
E-mail address: razykov@uzsci.net (T.M. Razykov).

0038-092X/$ - see front matter © 2010 Elsevier Ltd. All rights reserved.
doi:10.1016/j.solener.2010.12.002

of modules by the deposition process and consequently cost reduction for large-scale terrestrial applications.

In this paper, we review the current status of the PV market and recent results on several leading types of solar cells, such as c-Si, pc-Si, and amorphous-Si (a-Si), and III–V, II–VI, and I–III–VI_2 semiconductors and their alloys and nano-PV.

2. Efficiency limits

The thermodynamic efficiency of various devices is of wide interest because of the relevance of this parameter for energy conversion. The classic limiting efficiency of a solar cell was analyzed by Shockley and Queisser (1961). They also established a model to describe the electrical behavior of the diode that constitutes the solar cell. This time, the model came from detailed balance arguments and, at first sight, does not give the same results as the standard model. According to Shockley and Queisser (1961), the thermodynamic efficiency for an ideal single-homojunction cell is ~31%. The efficiency of a single-junction device is limited by transmission losses of photons with energies below the bandgap and thermal relaxation of carriers created by photons with energies above the bandgap.

In the classic case, every photon absorbed in a solar cell produces at most one electron–hole pair. Kodolinski et al. (1993) showed quantum efficiencies higher than 1 in the short-wavelength range of a-Si solar cell. This can be explained as an optically induced Auger mechanism: the energy in excess of the bandgap that one of the carriers receives from a high-energy photon is used in a second electron–hole generation. This result has led to the revision of the Shockley–Queisser model of the ideal solar cell, widely accepted as the physical limit of PV conversion.

Several methods have been offered to increase the power conversion efficiency of solar cells, including tandem cells, impurity-band and intermediate-band devices, hot-electron extraction, and carrier multiplication, the so-called "third-generation" PV (Nozik, 2002; Ross and Nozik, 1982; Hanna and Nozik, 2006; Green, 2002; Luque and Marti, 1997; Marti et al., 2006; Schaller and Klimov, 2004, 2006; Tobias and Luque, 2002).

The intermediate-band solar cell (IBSC) relies on the electronic and optical properties of so-called intermediate-band (IB) material, which is characterized by the existence of a collection of energy states located within what would otherwise be the forbidden bandgap of a conventional semiconductor. Normally, energy levels within a semiconductor bandgap are considered as non-radiative recombination centers. However, for ideal operation of the IBSC, these intermediate levels must behave only as radiative recombination centers. Thus, Marti et al. (2006) refer to this collection of levels as an intermediate "band." Radiative recombination can dominate when the wavefunctions of the electrons in the IB are delocalized (i.e., they extend throughout the crystal), as in the conduction and valence bands of conventional semiconductors.

To manufacture an intermediate-band solar cell, the IB material has to be sandwiched between conventional p- and n-type semiconductor emitters that isolate the IB from the contacts. When the device is illuminated, above-bandgap radiation pumps electrons from the valence band (VB) to the conduction band (CB), as in a conventional semiconductor solar cell. In addition, below-bandgap energy photons are able to pump electrons from the VB to the IB and from the IB to the CB. This requires the IB to be partially filled with electrons and implies that the Fermi level has to cross it.

The absorption of below-bandgap energy photons enhances the photocurrent over an ideal single-gap solar cell manufactured from material with the same bandgap E_g. In addition, the carrier population in each band is assumed to be governed by its own quasi-Fermi level (E_{Fc}, E_{Fv}, and E_{Fi} for the quasi-Fermi levels of the conduction, valence, and intermediate bands, respectively). The output voltage is then preserved because it is determined by the quasi-Fermi level split between the conduction and valence bands at the emitters, which is limited by the total bandgap E_g. As a result, the limiting efficiency of the IB solar cell is as high as 63.2% under maximum sun concentration (46,050 suns).

A single-threshold quantum-using device in which the exited carriers thermally equilibrate among themselves, but not with the environment, can convert solar energy with an efficiency approaching that of an infinite-threshold device. Such a hot-carrier flat-plate device operated under typical terrestrial conditions (AM 1.5 illumination, 300 K) can convert solar energy with an efficiency of 66% (Ross and Nozik, 1982). This high efficiency is achieved in part through an unusual inversion, in which the chemical potential of the exited electronic band is below that of the ground band. This negative potential difference reduces radiation losses, permitting a low threshold energy and a high Carnot efficiency, resulting from a high carrier temperature.

Another option to increase the efficiency of solar cells is that of using the carrier multiplication effect. Carrier multiplication, which was first observed in bulk semiconductors in the 1950s, would provide increased power conversion efficiency in the form of increased solar cell photocurrent. The process of inverse Auger recombination or impact ionization, as it is more commonly known, has also been considered as a mechanism to use some of the excess energy of photo-generated carriers to create additional electron–hole pairs in PV devices. When carrier multiplication is active, the effective photon-to-pair generation quantum yield may be greater than 1 for photon energies greater than twice the bandgap. The predicted limiting efficiencies are 44.7% and 85.9% for devices with maximum multiplication under unconcentrated and fully concentrated (blackbody) sunlight, respectively (De Vos and Desoete, 1998). Impact ionization is inefficient in typical bulk semiconductors such as silicon, and calculations show only marginal improvement in efficiency over the Shockley–Queisser limit. Very efficient multiple-exciton generation has been observed in quantum dots made from the

lead salts PbSe, PbS (Schaller and Klimov, 2004; Ellingson et al., 2005), and PbTe (Murphy et al., 2006) and from CdSe (Schaller et al., 2005). Schaller et al. (2006) have shown that for a PbSe quantum dot with a bandgap of 0.636 eV, up to seven excitons are created after absorbing a 5-eV photon, which corresponds to $7.8E_g$.

The purpose of a multi-junction device is to capture a larger fraction of the solar spectrum while minimizing thermalization losses. By stacking cells in the order of their bandgaps, with the cell with the largest bandgap at the top, light is automatically filtered as it passes through the stack, ensuring that it is absorbed in the cell that can convert it most efficiently. Another elegant simplification is that if bandgaps are appropriately selected, all of the cells in the stack will generate close to the same current, so the cells can be simply interconnected in series. The multi-junction concept was considered theoretically in the case of ideal cells operating in the radiative limit, to ascertain the maximum efficiency of photovoltaic conversion (Pauwels and de Vos, 1981; De Vos and Pauwels, 1981; Araujo and Marti, 1994; Marti and Araujo, 1996; Tobias and Luque, 2002). The highest-efficiency solar cells known are multi-junction cells based on GaAs and related group III–V materials. These cells are expensive for large-scale applications, but are usually used at the focus of mirrors or lenses that concentrate the solar light by a factor of 50–1000. A multi-junction cell with a large number of cells in the stack can theoretically approach 68.5% efficiency, as shown in Table 1 (Tobias and Luque, 2002). An edge-illuminated multigap PV system should show an efficiency greater than that obtainable with only a single gap. The theoretical upper limit to the efficiency will occur as the number of different gaps goes to infinity. For this case, a detailed balance limit analysis shows that at one sun the predicted efficiency is 64%, increasing with intensity to 81% at 10,000 suns.

Continuously increasing demand for PV modules and the need for low-cost PV options have stretched these advantages to the limit and have exposed some inherent disadvantages of c-Si technology, such as the scarcity of feedstock material, costly processing of materials and device fabrication steps, as well as the inability for monolithic interconnections. These, in turn, restrict the potential of Si wafer technology and it appears difficult to achieve PV module production costs below $1/W, which is considered essential for cost-competitive generation of solar electricity. The PV module cost depends on the total manufacturing cost of the module per square area and the conversion efficiency. Fig. 1 (Green, 2002) gives an estimate of

Table 1
Thermodynamic efficiency limits (unconcentrated sunlight).

Number of junctions	Efficiency (%)	E_g (eV)
1	40.6	1.06
2	55.6	1.63–0.74
3	63.6	2.02–1.21–0.59
4	68.5	2.31–1.55–0.99–0.5

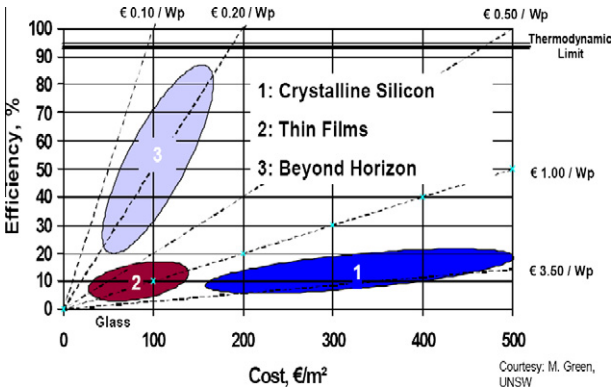

Fig. 1. Cost-efficiency analysis for first-generation (1), second-generation (2), and third-generation (3) photovoltaic technologies.

achievable cost with c-Si technology and comparison with projected achievable costs with other PV technologies. It is generally agreed that c-Si wafer technology would not be able to meet the low-cost targets, whereas thin-film technologies have the potential to provide a viable alternative in the near future.

The so-called "third-generation PV" will be based on nanostructures. An important advantage for nanostructured solar cells is that they can be used to incorporate new physical mechanisms that allow an efficiency greater than that of a one-junction solar cell. Nanostructured solar cells offer several advantages for solar cells, including: (1) the ability to exceed a ingle junction solar cell efficiency by implementing new concepts, (2) the ability to overcome practical limitations in existing devices, such as tailoring the material properties of existing materials or using nanostructures to overcome constraints related to lattice matching, and (3) the potential for low-cost solar cell structures using self-assembled nanostructures.

3. PV market

The rapid growth of the PV market began in the 1980s due to the application of multi-megawatt PV plants for power generation. The present PV market grows at very high rates (30–40%), similar to that of the telecommunication and computer sectors. World PV production in 2009 increased to 10.66 GW (Fig. 2) (Maycock, 2010). This became possible owing to technology cost reduction and market development, reflecting the increasing awareness of the versatility, reliability, and economy of PV electric supply systems. Major market segments served by this industry comprise consumer applications, remote industrial systems, developing countries, and grid-connected systems. Of particular interest is the strong differential growth rate in rural applications, which now accounts for nearly half of the total PV market. The second largest market is industrial applications.

PV applications are progressively finding their markets mainly in the United States, Japan, and the European

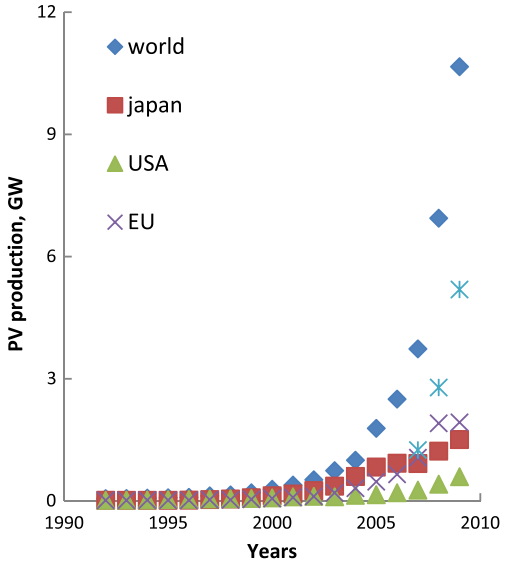

Fig. 2. Evolution of world PV cell/module production through 2009.

Union (mostly Germany) and China/Taiwan. The annual production of PV cells and modules in the United States, Japan, European Union, and China/Taiwan in 2009 was 595 MW, 1.5 GW, 1.93 GW, and 5.19 GW, respectively. Recently, China/Taiwan became the leading PV country, and PV production has almost doubled (Table 2).

According to Maycock (2010), another 6.9 GW of cell and 6.7 GW of module capacity is being added—most of it in China, Taiwan, and Japan—bringing total global cell and module capacity to 25.1 GW and 22.7 GW, respectively. This goal cannot be achieved on wafer Si only because of an expected Si shortage, despite a large annual production of semiconductor-purity Si, which is 30.000 tons/year. Quick penetration of the second-generation PV (thin-film solar cells) into the world PV market is therefore required.

The top 10 producers of PV cells and modules are presented in Table 2. These companies produced 4.92 GW in 2009, which amounts to almost 50% of world production.

In terms of technology, c-Si and pc-Si wafers are the main materials for the world PV industry (Table 3) (Maycock, 2010). At the present, over 80% of the world PV industry is based on c-Si and pc-Si wafer technologies. The CdTe technology is growing sufficiently fast, while thin-film CIGS and a-Si-based PV production is still in the beginning stages, despite the remarkable results of R&D many years ago. This may be due to difficulties between laboratory and large-scale production technologies. Several new multi-megawatt thin-film plants are ready for production of these types of solar cells, and their contribution to the world PV market might be significantly

Table 3
2009 World PV cell production by technology (MW).

c-Si	CdTe	CIGS	a-Si
8.678	1.019	166	796

expanded soon. It is expected that thin-film PV technologies will play a major role in the world PV market in the near future.

At present, the PV market is dominated (more than 40%) by grid-connected residential systems. Module prices are in the range of US$ 3.0–4.5/W_p, and the system prices are in the range of US$ 5–7/W_p, depending on technology and size. According to the US Department of Energy targets, the cost of energy is US$0.06/kW h for utility, US$ 0.08/kW h for commercial, and US$ 0.10/kW h for residential applications by 2015.

4. Silicon solar cells

4.1. Crystalline Si solar cells

Most commercial Si solar cells have used boron-doped single-crystal wafers (around 400 μm thick) grown by the Czochralski (CZ) process. It is the standard process used for the needs of microelectronics. CZ Si is free from lattice defects; however, it contains residual impurities such as oxygen, carbon, and transition-metal ions. Oxygen introduced from a quartz crucible is beneficial for microelectronics, because the oxygen strengthens the wafers and can also be used for guttering defects from wafer surfaces. Oxygen reacts with the boron to form an electronically active defect that limits the quality of the material after illumination (Green et al., 2001). Magnetic confinement is used to reduce the amount of oxygen by transferring material from the crucible within the melt. Si grown by the float-zone (FZ) process is the preferable method for solar cells of highest efficiencies because it has the lowest recombination losses. FZ Si with diffusion lengths up to 800 μm for 1 Ωcm material can be produced.

The evolution of world-record efficiencies of laboratory cells is shown in Fig. 3. Si cell efficiency can be divided into four stages, with each stage corresponding to new solutions in technology or cell structure. In the beginning of the "semiconductor era" (after the discovery of the bipolar transistor in 1948), the rapid progress of silicon technology allowed production of Si solar cells with 15% efficiency. In the second stage (1970s), 17% efficiency Si solar cells were fabricated due to achievements in microelectronics (e.g., photolithography). The most significant results have been obtained in the third (1980s) and fourth (2000+) stages,

Table 2
Top 10 PV cell/module producers, 2009 (MW).

First Solar	Suntech Power	Sharp	Q-Cells	Yingly Green Energy	JA Solar	Kyosera	Trina Solar	Sunpower	Gintech
1.011	704	595	537	525	509	400	399	398	368

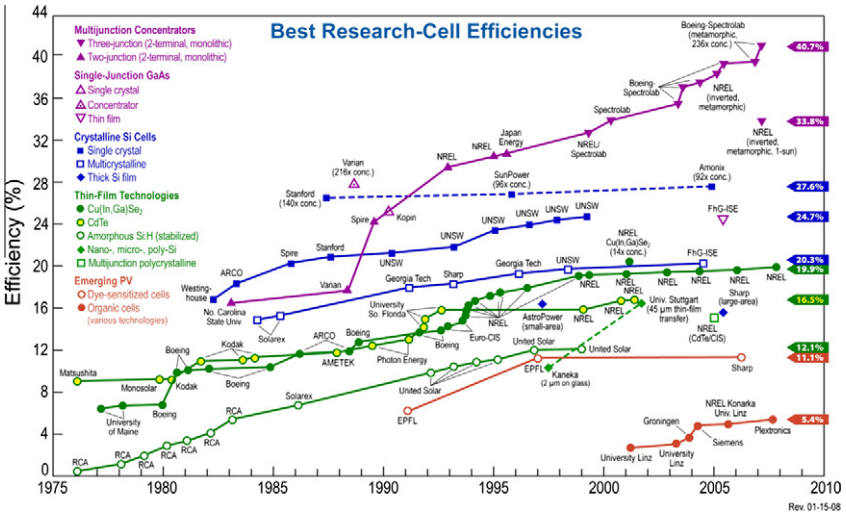

Fig. 3. Evolution of the conversion efficiencies of various types of research PV cells.

and Si cell efficiencies close to 25% have been achieved. These efficiencies were due to improved contact and surface passivation of the cell, along the front and rear surfaces, as well as an improved understanding of the significant role of light-trapping in Si devices (Green et al., 2001). For Si cells 80 μm thick, the maximum efficiency is 28.8%.

The main features of Si solar cells were noted in Wettling (1995) and Green, 2000a,b. Optically, the inverted pyramids on the top surface significantly reduce reflection loss. The metal rear contact serves as an efficient reflector. Consequently, light is very effectively trapped within the cell up to 40 times (Green, 2000a,b). For low-quality wafers, the buried-contact cells become less important because the open-circuit voltage is dominated by recombination in the bulk regions of the cells rather than at the contacts. The passivated emitter and rear, locally diffused (PERL) cell on a FZ wafer has achieved 24.7% efficiency (open-circuit voltage $[V_{oc}] = 706$ mV, short-circuit current density $[J_{sc}] = 42.2$ mA/cm^2, and fill factor [FF] = 0828), which is the highest efficiency reported for a-Si solar cell (Zhao et al., 2001). Commercial c-Si cells have efficiencies in the range of 15–22%.

4.2. Polycrystalline wafer Si solar cells

pc-Si wafers can be fabricated over large areas. Plasma processing of lower-cost pc-Si is used to form a highly transmissive surface and to increase the light absorption. Known as reactive-ion etching, this process allows about a 40% relative increase in absorption. The importance of texturing pc-Si to reach its full potential was considered by Zolper et al. (1989) and Inomota et al. (1996). 19.8%-efficienct textured pc-Si solar cells have been fabricated (Zhao et al., 1998). Bulk hydrogenation and nitride passivation of the cell surface have produced good results. Despite a number of advantages of pc-Si, there is no significant difference between the costs of c-Si and pc-Si solar cells. Commercial pc-Si cells have efficiencies of 12–15%.

4.3. Thin-film c-Si and pc-Si solar cells

Thin-film Si solar cells have the following important advantages compared to crystalline cells: (i) The thickness of Si can be drastically reduced to 50 μm; (ii) Thin films can be deposited on low-cost substrates; (iii) Thin films can be fabricated on module-sized substrates and in integrally interconnected structures. According to some calculations, the thickness of Si films can be reduced down to 1 μm (Green et al., 2001).

Although Si films were developed in microelectronics many years ago, it has taken about 30 years to begin fabricating thin-film pc-Si solar cells with reasonable efficiency. The technology developed by Basore (2004) involves the direct deposition of silicon onto glass, followed by solid-phase crystallization—a thin-film approach called Crystalline Silicon on Glass (CSG)—and a mini-module with 8.0% efficiency was fabricated.

The best Si-based solar cell efficiencies are presented in Table 4. Continuous poly-Si films on glass substrates were obtained by Ebil et al. (2004), using an *in situ* aluminium-induced crystallization technique at 430 °C. Poly-Si films had an average grain size of 10–15 μm, corresponding to a grain size/thickness ratio of greater than 20. The status of this field in the USA has been reviewed by von Roedern (2003). A cell with a thickness of 2.0 μm has demonstrated an efficiency of 10.7% (Yamamoto et al., 1999). Thus, this field is in the initial stage.

Table 4
Best Si solar cells efficiencies.

Device	Efficiency (%)	Reference
c-Si (wafer)	24.7	Green (2000a)
pc-Si (wafer)	19.8	Inomota et al. (1996)
c-Si (thin film)	8.2	Zhao et al. (1998)
a-Si (thin film)	13.7	Hamakawa (1994)

4.4. Thin-film amorphous- and nano-Si solar cells

Thin a-Si films usually contain a few percent of hydrogen to passivate dangling bonds and increase material quality. Plasma chemical vapor deposition (CVD) is widely used for fabricating these films. The design of the cells optimizes the collection of current by having very thin n- and p-layers, with an intrinsic intermediate layer—the thickness of which is enough to absorb almost all the incident light—to give a p-i-n structure. However, the physical properties of the i-layer degrade under illumination, because Si-H bonds are destroyed under visible light. This effect can be reduced (but not eliminated) by careful control of the deposition process, decreasing the thickness of i-layer, and using multiple junctions (Hamakawa, 1994). The best initial efficiencies of 13.7% and 9.8% were achieved on triple-junction cells and modules, respectively, many years ago (Guha, 1992). However, stabilized efficiencies still remain low: 6–7% for the best commercial modules (Table 5) (von Roedern et al., 2005). Nevertheless, at present, about 8–10% of the worldwide PV production uses a-Si technology.

4.4.1. Material and properties

The oil crisis of the early 1970s gave an impetus to PV R&D activities, and several concepts for thin-film PV started to emerge. The first report on thin-film a-Si-based solar cells appeared in 1976 (Carlson and Wronski, 1976). Indoor consumer products began appearing in the market in the 1980s, although it took quite some time to understand the basics of the material and device properties and their inherent bottlenecks. Amorphous-Si is now the most studied and applied material for thin-film solar cells, compared to its counterparts. Silicon has the advantage of being an abundant material in the Earth's crust, and so following the trends of c-Si technology, a-Si developed over the years into an industrially mature technology (Rech and Wagner, 1999). Besides, a-Si has several other non-PV applications that provided it with additional importance.

Crystalline Si has long-range atomic ordering extending up to a few cm within single crystals, whereas a-Si has short-range atomic ordering of less than 1 nm, and thus the material is not a crystal. Amorphous silicon has a disordered lattice showing localised tetrahedral bonding schemes, but with broken Si–Si bonds of random orientation, as shown in Fig. 4. These broken (or unsaturated) bonds are called "dangling bonds" and they contribute to the defect density in the material. Because of disorder, the momentum conservation rules are relaxed and a higher absorption coefficient (α) has resulted in a-Si material. The absorption coefficient of a-Si is about two orders of magnitude higher than c-Si; thus, it requires a thickness of only a couple microns for effective absorption and use of the solar spectrum. However, due to its predominant disordered structure, a high density ($\sim 10^{19}\ cm^{-3}$) of localised defect states are created within the energy gap, causing Fermi level pinning; hence, the material cannot be doped because the defect states act as traps for all free carriers generated in the material.

One effective way to overcome this problem is to passivate the unsaturated bonds of a-Si with the help of small-diameter atoms that can enter into the crystal and attach themselves with the available bonds. This is precisely done by adding 5–10% atomic hydrogen into a-Si, and the hydrogen attaches itself to the uncoordinated bonds due to its high activity, thus reducing the dangling bonds density from $\sim 10^{19}$ to $\sim 10^{15}\ cm^{-3}$. At this order of defect density, doping is possible, and hence, the material can be made p- or n-type using boron and phosphorous, respectively, as dopants. However, the defect density still remains so high that even with high doping, the Fermi level does not move away too much, remaining mostly within the donor and defect levels at the center of the gap in the case of n-type doping.

Amorphous silicon may be considered as an alloy of silicon with hydrogen. The distortion of the bond length and bond angle after passivation with hydrogen modifies the defect distribution and consequently changes the optical and electronic properties. Many studies have found that by changing the deposition conditions, hydrogen-diluted microcrystalline Si (μc-Si) can be obtained that has rather different properties (Vetterl et al., 2000; Guha et al.,

Table 5
Best large-area thin-film modules.

Company	Device	Size (cm^2)	Efficiency (%)	Power (W)	Date
Mitsubishi Heavy[a]	a-Si	15,625	6.4 (stabilized)	100	7/05
Global Solar Energy	CIGS	8709	10.2	88.9	5/05
Wurth Solar	CIGS	6500	13	84.6	6/04
United Solar	a-Si	9276	7.6 (stabilized)	70.8	9/97
First Solar	CdTe	6624	10.2	67.4	2/04
Shell Solar GMBH	CIS	4938	13.1	64.8	6/04
Sharp[a]	nano-Si	4770	11 (stabilized)	52.5	7/05
Antec Solar[a]	CdTe	6633	7.3	52.3	6/04
Kaneka	a-Si	8100	6.3 (stabilized)	51	7/04
Shell Solar Industries	CIS	3644	12.9	46.8	5/05
Showa Shell[a]	CIGS	3459	13.4	46.45	8/02
EPV	a-Si	7432	5.7 (stabilized)	42.3	10/02

[a] Reported by company, but not independently measured.

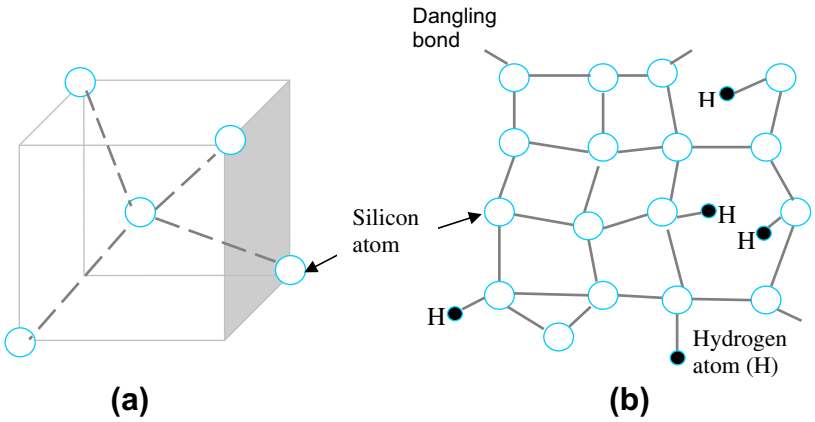

Fig. 4. Tetrahedral bonding scheme in crystalline Si (a) and network of a-Si:H exhibiting broken silicon atom dangling bonds, which are passivated by hydrogen atoms (b).

1981, 1986; Matsuda et al., 1986). Fig. 5 compares the absorption coefficient of a-Si:H, c-Si, and μc-Si, along with other PV materials. The absorption bands (plateau) appearing at low energy values for a-Si:H and μc-Si are ascribed to the presence of large-density mid-gap defects and band-tail states. The absorption coefficient (α) of monocrystalline Si wafers and microcrystalline thin-film Si have the same onset of transition, but μc-Si has a higher α in the low-wavelength (λ) region. However, α for μc-Si is lower than that of a-Si; therefore, thicker μc-Si layers are required for effective absorption of the solar spectrum compared to a-Si. A stacked combination of the two—microcrystalline and amorphous-Si layers—is attractive for absorption of the most useful part of the spectrum in thin layers. This has been successfully employed first by IMT (Neuchatel, Switzerland) and later by several other groups to develop a-Si/μc-Si tandem (also often called "micromorph") solar cells.

The bandgap of a-Si can also be tailored by adding O, C, and Ge to produce amorphous materials of wider or narrower bandgaps (e.g., with addition of C and Ge in a-Si:H, bandgaps of 2.2–1.1 eV are achievable, but with inferior electronic properties). Table 6 provides a list of these alloys, with their respective bandgaps. Suitable a-SiC:H and a-SiGe:H for solar cell devices have bandgaps of ~2.0 and 1.3 eV, respectively.

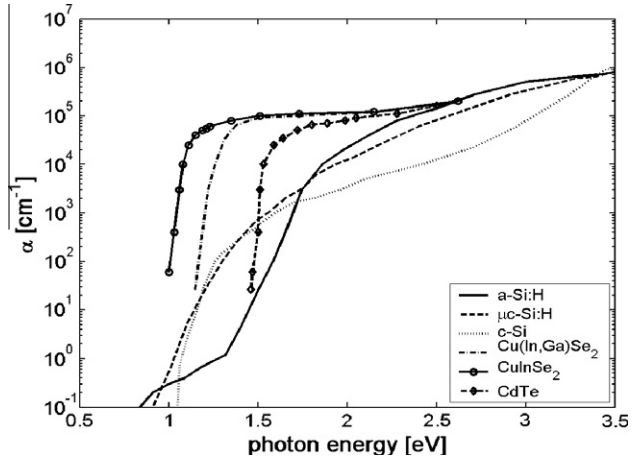

Fig. 5. Optical absorption (α) versus bandgap (E_g) spectra of c-Si and other prominent light-absorbing materials used in thin-film solar cells.

4.4.2. Deposition techniques

Perhaps the most important feature of a-Si material is that a wide range of temperatures (from room temperature to 400 °C) can be used for deposition. Room-temperature deposition allows the use of a variety of substrates (e.g., glass, metal, plastic), and, in particular, the possibility of using low-cost plastic polyethylene terphthalate (PET), which could be a significant advantage in reducing the cost of the modules. There are various processes used for depositing a-Si:H material. Silane (SiH_4), which is the basic precursor gas, is used in nearly all processes using the CVD method, but excluding sputtering, which is not preferred for active semiconductor layers in a-Si:H. The typical deposition temperature for a-Si:H must be below 500 °C; otherwise, the incorporation of hydrogen in the film is not possible. At low substrate temperatures, the predissociation of SiH_4 does not occur easily. Hence, room-temperature-deposited layers give rise to inferior quality and efficiency. Therefore, plasma is used for dissociation of silane gas. The two most commonly used methods for dissociation are plasma-enhanced chemical vapor deposition (PECVD) and glow-discharge CVD. Typically, 13.56-MHz plasma excitation frequencies with optimal

Table 6
Energy bandgaps (E_g) of certain alloys of a-Si:H with Germanium and carbon used in multi-junction solar cell structures.

Material (semiconductor/alloy)	E_g min (eV)	E_g max (eV)
c-Si	1.1	1.1
μc-Si:H	1.0	1.2
a-Si:H	1.7	1.8
a-SiC:H	2.0 (in 20% C)	2.2
a-SiGe:H	1.3 (in 60% Ge)	1.7
a-Ge:H	1.1	

plasma excitation power at 0.1–1 mbar pressure are used. SiH_4, always diluted with hydrogen (~10%), is used to deposit a-Si:H, whereas increasing hydrogen dilution results in μc-Si:H layers, but with lower growth rates. The typical deposition rates for a-Si cells (in R&D) is ~1 Å/s and results in fairly long deposition times (50 min for a 0.3-μm-thick a-Si:H cell and 5 h for a 1.8-μm-thick μc-Si:H cell, whereas 3 Å/s or higher deposition rates are generally preferred in production plants. For high deposition rates, technologies based on very high-frequency (VHF), microwave and high-pressure plasma are currently being pursued at the R&D level. Rates as high as 10 Å/s have been achieved at laboratory scale. Alternative deposition methods using the hot-wire CVD technique (HWCVD), electron cyclotron resonance reactor (ECR), and also the combination of HWCVD and PECVD are also being carried out to increase the deposition rate. A detailed account of some of these techniques can be found in the Lechner and Schade (2002), Sopori (2003), Deng and Schiff (2003), and Klein et al. (2004).

4.4.3. Amorphous silicon solar cells and configurations

The conventional p–n junction configuration for a-Si:H-based solar cells suffers from various inherent limitations due to the presence of a large number of defect states, even after H-passivation. The doping of a-Si:H further increases this concentration, which reduces the average lifetime of the free carriers as a result of very high recombination probabilities and low diffusion lengths of ~0.1 μm; thus, solar cells in the p–n configuration do not work and are not considered suitable. The basic structure of an a-Si solar cell configuration is a "p–i–n" junction, shown in Fig. 6a, which illustrates qualitatively the thickness of different layers in the device in the "superstrate" configuration with applied texturing (roughness) of the transparent conducting electrodes for enhanced light-trapping in the a-Si layer, as described later.

The p–i–n type configuration (Fig. 6b) for the a-Si solar cell was introduced by Carlson et al. at RCA Laboratories (USA) (Carlson and Wronski, 1976), where an intrinsic layer of a-Si:H is sandwiched between the n- and p-type doped layers of a-Si:H or its alloys. Because of the very short lifetime (or high recombination) of the carriers, the doped layers do not contribute to the photocurrent generation (the photons absorbed in these layers contribute to optical losses); but these p- and n-layers build up the electric field across the i-layer. This electric field drives the electrons and holes photo-generated in the i-layer in opposite directions, so that the i-layer essentially acts as the absorber layer in a-Si:H solar cells. The electrical field depends on the doping concentration of p- and n-layers, as well as the thickness of the i-layer. Because the p- and n-doped layers do not contribute to photocurrents and can cause further recombination of the generated carriers before sweeping across the layer, it is essential to minimize their thickness, which is typically ~10–30 nm. There is an upper limit to the thickness of the i-layer (~0.5 μm), because charge defects reduce the effective field, and thus, if the width of the i-layer exceeds the space-charge width, then the extra width would act as a "dead" layer without actually contributing to photocurrent.

4.4.3.1. Stability and recombination issues in a-Si solar cells. The initial results of a-Si cells in the 1970s indicated very promising potential for attaining efficiencies well above 10%. However, it was soon observed and realized that a-Si solar cells suffer from an inherent problem of light-dependent degradation on their performance under continuous light exposure, attributed to the Staebler–Wronski Effect (SWE) (Staebler and Wronski, 1977). It was observed that in a timescale of a few months, the performance of the cells dropped about 30–40%, then stabilized at an efficiency lower than the initial value. This initial drop in performance is significant and takes the edge off the

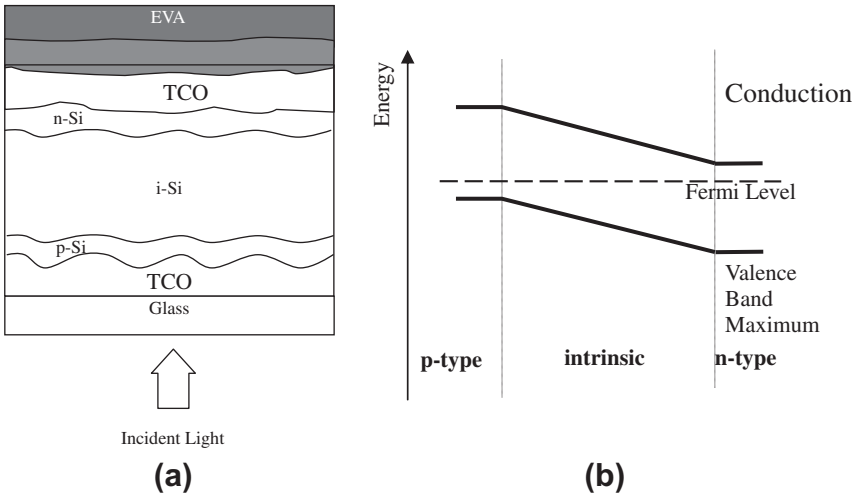

Fig. 6. (a) Single-junction a-Si solar cell in superstructure configuration; EVA is the polymer coating used for encapsulation of solar cell. (b) Energy band diagram of p–i–n solar cell structure.

promise shown by this cheaper alternative to c-Si technology. The drop keeps the a-Si cell much below the efficiency threshold limit (generally accepted as ~10% module efficiency for thin-film vacuum-based technologies). An explanation for the light-induced degradation is that with light exposure, the Si–H bonds break and further increase the density of the dangling bonds. Thus, the system is driven into an excited or higher energy state, with active defect centers leading to higher recombination of the free carriers and hence a reduction in efficiency. The efficiency drop depends on the illumination level and operating temperature of the solar cell. It has been observed that efficiencies may be partially recovered by heating the cells. The heating recovery depends on the temperature of the cells; for instance, annealing at 70 °C helps in stabilising the system better than at room temperature.

The control of defect (trap) states and dangling-bond passivation for effective doping of the a-Si:H layers are significant in the a-Si cell's overall design. The first inherent problem of the technology is that SWE cannot be eliminated, but can only be reduced by engineering of the device's structure (e.g., by employing a thinner i-layer at the expense of absorption loss). Several groups have verified that efficiency degradation is lower in solar cells and modules with thinner i-layers. The second problem is that the doping of the a-Si leads to an increase of trap density, leading to pronounced recombination effects in the device; therefore, limiting the thickness of the doped layers to 10–30 nm for minimized recombination effects. The limits on i-layer and n- and p-doped layer thicknesses together have a direct bearing on the overall device structure and performance stability.

4.4.3.2. a-Si solar cell configurations. An advantage of a-Si is that the solar cells can be grown in both "superstrate" and "substrate" configurations, as shown in Fig. 7. In the "superstrate" configuration, the cell is grown in the p–i–n sequence (starting with the p-layer, followed by i- and n-layers) onto a substrate that must be transparent (such as glass); hence, this configuration is not suitable for metal or highly opaque polymeric substrates. In conatrast, the "substrate" configuration can be grown on any type of substrates, which could be rigid glass or flexible metal or polymer foil. It bears an n–i–p configuration (cell growth starting with n-layer followed by i- and p-layers) and the light enters through the last grown p-layer.

Generally, a-Si solar cells on glass are available in the superstrate configuration starting with a transparent conducting oxide (TCO) window, then having p–i–n layers grown on it, followed by another TCO layer and a metallic back-reflector layer. One of the leading US-based companies, United Solar (USOC, formerly USSC) has been using the substrate configuration for roll-to-roll production of cells on stainless steel (SS) and polymer foils. The layers can be grown in n–i–p or p–i–n sequence. But irrespective of the substrate or superstrate configuration, incident light is allowed through the p-side, because it has a higher bandgap than the i- or n-layers. Also, because the mobility of holes is smaller than compared to electrons, a thin front p-layer supports hole collection in the device (Rech and Wagner, 1999).

The choice of TCO material, as well as its electrical and optical properties, is important for electrical contacts but also for efficient light-trapping through the device. Light-trapping is essential for efficient performance of a-Si solar cells, where device thickness is limited by several inimical factors, e.g., thinner i-layer is desired for minimizing light-induced performance degradation. Consequently, the thickness of the intrinsic layer, which acts as an absorber, is generally limited to only ~300 nm, which is not sufficient for absorption of a large part of the solar spectrum. To effectively use the incident photons, the applied strategies must reduce the reflection by using refractive index grading for the entire spectral wavelength range cell response and by allowing multiple scattering of light for enhanced absorption of photons in the i-layer. Reflection is reduced by an antireflection coating on the glass, where the light enters into the PV module, and by suitable surface

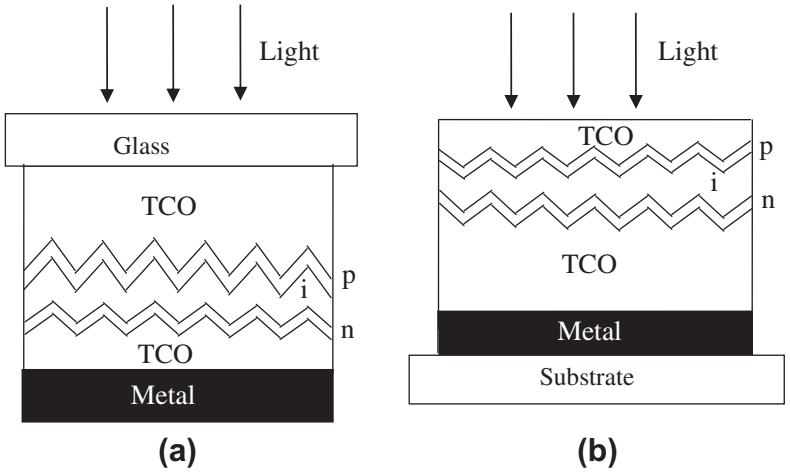

Fig. 7. (left) a-Si solar cell in "superstrate" (p–i–n) configuration, and (right) "substrate" (n–i–p) configuration.

texturing of the TCO with feature sizes comparable to the wavelength of the light. Multiple light scattering is achieved by the application of metal reflectors. For detailed descriptions of TCOs and light scattering, see Goetzberger et al. (2003) Muller et al. (2004), Granqvist (2003), and Shah et al. (2004). TCOs such as SnO_x:F, indium tin oxide (ITO), and ZnO:Al have been extensively used in a-Si solar cells. Some requirements for good a-Si:H solar cells are the following:

- Glass and front TCO should have a high (>80%) transparency over the whole spectral range.
- TCO with a sheet resistance of at most 10–15 Ω/square (high conductivity) obtained by enhancing carrier mobility rather than the carrier concentration to minimize free-carrier absorption over the near-infrared region.
- TCO layers and doped silicon layers, which do not contribute to photo-generation and collection, should be kept as thin as possible and have very low absorption coefficients.
- TCO layer should not degrade by chemical reduction during a-S:H deposition.
- Use of back reflectors with as little absorption as possible.

The properties of doped and intrinsic layers have been widely studied and layers are employed in optimised conditions. However, light-trapping through various structures and patterns are relatively recent advancements and thus open up more possibilities for improving device performance (Muller et al., 2004; Granqvist, 2003). In the following sections, we discuss other innovations for improving efficiency and stability that relate to device architecture by using tandem or multi-junction and hetero-junction cells.

4.4.3.3. Multiple-junction or tandem solar cells. Light-induced degradation has become the biggest bottleneck of the a-Si technology, and it has serious implications. The general effects of high density of trap and recombination centers have restricted the thickness of the device layers, which consequently limits the absorption of the incoming light. The clever p–i–n configuration once thought to have great promise for high efficiency at lower cost was also hindered by this instability issue. Tandem cells using double and triple junctions have been thoroughly pursued worldwide to work within the limits of an i-layer thickness of ~300 nm and using different light-trapping arrangements. Single-junction a-Si solar cells are rarely used today because of low efficiency and stability problems. Multi-junction solar cells are used for better use of the solar spectrum and to improve stability. The stabilized efficiency (small area) for single-junction cells is 9.3%, whereas it is 12.4% for double-junction and 13.0% for triple-junction cells using a-Si:H and its alloys (Guha, 2004). Fig. 8 presents schematics of different multi-junction structures. The development of multi-junction solar cells is based on the following strategies:

(i) The first strategy is based on using only a-Si:H intrinsic layers. Such double-junction devices have been developed by Fuji Electric & Co. (Japan) and Phototronics (Germany) (part of RWE Schott), and others. Stabilized laboratory efficiencies are ~8.5%, and modules with about 5.5% efficiency are commercially available (Diefenbach, 2005).

(ii) The second strategy includes using a-Si and Ge alloys with different bandgap combinations (lower than 1.7 eV) to form tandem junctions, where the top cell is 1.7-eV a-Si:H-based and bottom cells have a-SiGe:H alloy layers of lower (1.5–1.3 eV) bandgaps. United Solar (USSC) has developed 13%-efficient

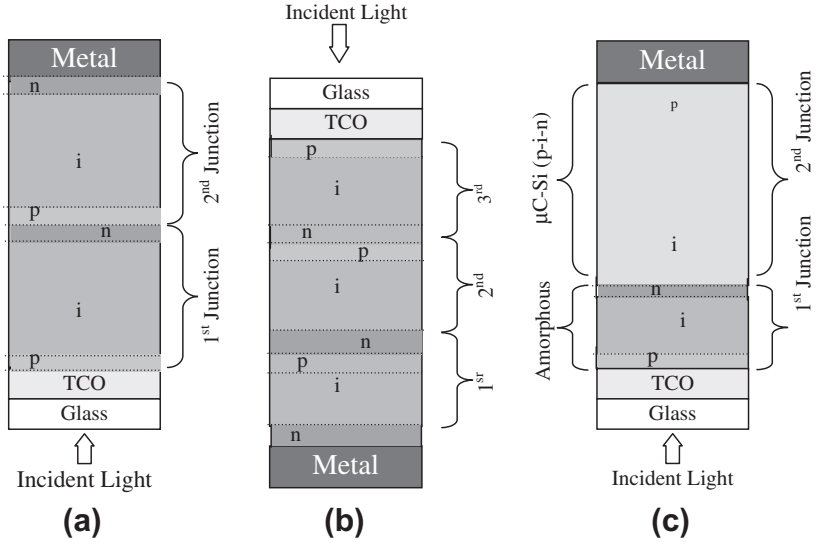

Fig. 8. Multi-junction cell architecture showing (a) double-junction "superstrate" configuration, (b) triple-junction in "substrate" configuration, and (c) "micromorph" junction in "superstrate" configuration; i.e., glass/TCO/p–i–n (a-Si:H) /p–i–n (μc-Si:H).

triple-junction solar cell (small area) in substrate configurations and is selling their triple-junction modules on stainless steel at stabilized efficiency of about 6.5%.

(iii) The third strategy, introduced in 1994 by IMT (Neuchatel, Switzerland), is based on a novel concept of combining μc-Si:H (with a bandgap of 1.1 eV) and a-Si:H (with a bandgap of 1.7 eV) based solar cells. This has promising potential because of the significantly reduced light-dependent degradation effect in a tandem solar cell (Shah et al., 2004). The only degradation observed comes from the a-Si layer, which is optimised at 0.2–0.3 μm, while the μc-Si layer is kept around 1–2 μm. Kaneka Corporation (Japan) has recently achieved large-area modules (910 mm × 455 mm) of initial efficiency ~13.2% and with stabilized efficiency approaching 10%. Using the concept of an intermediate TCO reflector layer for novel light-trapping, Yamamoto et al. (2004) have shown an initial efficiency of 14.7% for a test cell. The reason for the high efficiency lies in the spectral response of the combination of 1.7-eV a-Si:H-based cells with 1.1-eV μc-Si:H-based cells. The superposition of the two results in a quantum efficiency spreading around 80% between 500 nm and 800 nm, covering a large part of the solar spectrum.

4.4.4. Hybrid solar cells

Amorphous silicon cells have been combined with nanocrystalline silicon-junction cells and cells of other materials such as CIGS. Another significant design development is the formation of a thick/thin type of interface structure (heterostructure) between the a-Si:H layer and the c-Si wafer. Developed recently by Sanyo, Japan, these cells are referred to as HIT cells—for Hetero-junction with Intrinsic Thin film layer cells. Their efficiency is close to 21% over a cell area of 101 cm^2. This technology uses an n-type CZ-silicon wafer as the base (light absorber) and low-temperature processes with a device structure of a-Si(p^+)/a-Si(i)/c-Si(n)/a-Si(i)/a-Si(n^+). The intrinsic a-Si layer is important because it contacts c-Si at both ends, and it provides passivation and extra stability to the system. The cells have exhibited excellent stability, and pilot-plant production by Sanyo is already under way.

4.4.5. Flexible a-Si solar cells and modules

4.4.5.1. Monolithic modules. All solar modules require a number of solar cells to be electrically connected in series to provide power, depending on size and cell efficiency. Additional processing steps such as attachment of leads and encapsulation for protection against external influences are done to finalize the module structure. The "superstrate" configuration has advantages for monolithic electrical interconnection of solar cells to form solar modules because the substrate (e.g., glass, polymer) is insulating. In contrast, in the "substrate" configuration, individual large-area solar cells are mechanically connected cell to cell, as done in c-Si technology. USSC, USA, follows this electrical contacting approach for triple-junction a-Si solar cells on steel foil.

Fig. 9 illustrates the monolithic interconnection scheme to develop solar modules in "superstrate" configuration. For interconnection of solar cells, layers are laser scribed in three stages: first to separate the front TCO contact, then scribing a-Si layers to connect individual cells, and finally to isolate the conducting back-electrode to obtain series interconnection. This approach removes the need for separating and connecting cells, which is time consuming, costly, and complex in conventional c-Si technology.

4.4.5.2. Flexible a-Si solar cells. Another important perspective of thin-film PV technology is flexible modules with strategic space and military use, integration in roofs and buildings facades, and use in portable power sources, automobiles, and consumer electronics. Since they can be made in different shades (even semi-transparent), shapes, and sizes, these flexible a-Si solar cells are likely to be very popular and in demand for applications in the low to medium range of power.

Some prominent companies currently involved in production and development of flexible a-Si-based modules are listed in Table 7. Of these, US-based United Solar,

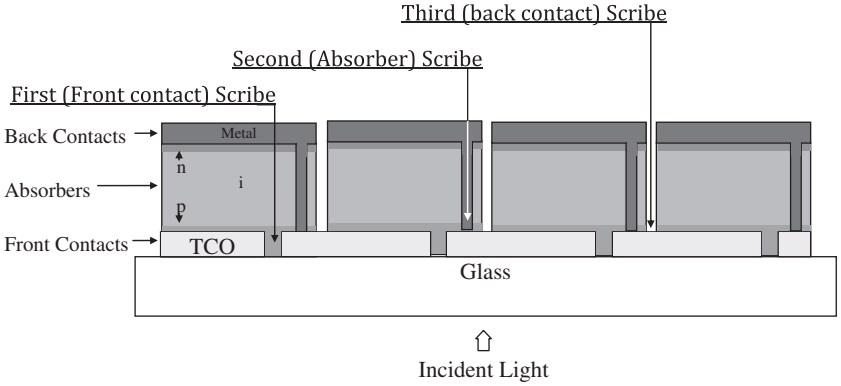

Fig. 9. Monolithic module design with single-junction a-Si cell in "superstrate" configuration. Similar strategy can also be used for modules on polymer foils or multi-junction solar cells, which may have different sequence of layers.

Table 7
Companies active in flexible a-Si thin-film Si PV. Generally, module efficiencies are in 3–8% range.

Companies	Technology	Production	Remarks
United Solar	Triple-junction SiGe alloys On stainless steel RF-PECVD	30 MW line, RF-PECVD, Modules and consumer products	Modules between 6.5% and 6.8% Cutting-assembling process Modules with 8% for military and space application
VHF-Technology	a-Si on PEN, polyimide VHF-PECVD	Pilot production and consumer products	Product efficiency ~4%
Iowa Thin-Film Technology (ITFT)	a-Si on polymide, RF-PECVD	Pilot production and consumer products	Product efficiency ~4%
Fuji Electric	a-Si/a-Si on polymide RF-PECVD	Pilot production and consumer products	Feed-through contacts through the substrates, 7% module, 8% active area stable efficiency
Sanyo	a-Si on plastic RF-PECVD	Consumer products	
Canon	μc-Si:H/a-Si:H on stainless steel (VHF-PECVD)	Development	
Akzo Nobel	Amorphous p–i–n on Al RF-PECVD	Development, pilot-line	Al sacrificial substrate dissolved after cell deposition

Iowa Thin Films, and Japanese companies like Sanyo and Fuji have entered into relatively large-scale production, while European companies Flexcell (Switzerland) and Akzo Nobel (the Netherlands) are starting pilot production plants for the consumer-oriented market. But it will need an efficiency above ~12% and long-term stable performance of large-area modules to make it compete effectively with c-Si. And to remain a leader among other thin-film options, low-cost modules must be developed with production processes that give high throughput and yield.

5. Thin-film chalcogenide solar cells

In the early 1960s, thin-film Cu_xS–CdS, Cu_xSe–CdSe, and Cu_xTe–CdTe solar cells were developed. Fabrication technology of these solar cells was very simple. CdS, CdSe, and CdTe films were fabricated by chemical vapor deposition. Cu_xS, Cu_xSe, and Cu_xTe layers were fabricated by dipping CdS, CdSe, and CdTe films into an aqueous solution of CuCl for a few seconds (Cusano, 1963; Lebrun, 1966). More than 10% efficiency was achieved for all three cells. However, research on these cells stopped because of degradation (copper diffusion) of copper chalcogenide layers. Nevertheless, R&D results revealed many physical processes in thin-film solar cells.

5.1. II–VI solar cells

5.1.1. CdTe cells

The basic properties of II–VI films are presented in Table 8. Cadmium telluride (CdTe) is a direct-bandgap material. Its bandgap energy of ~1.45 eV is quite favorable for conversion of the solar spectrum into electricity with a single-junction solar cell. Its very high optical absorption (10^5 cm^{-1}) and p-type conductivity make it an ideal material for PV applications. It has a "zincblende" crystal structure and a simple phase diagram as the constituents have high vapor pressure. The layers of CdTe can be deposited using a number of processes, and the compound can easily be grown in stoichiometric form at temperatures over 400 °C. As with other II–VI materials, electronic doping is controlled by substitution of atoms at vacancy sites. Although n-type doping control is relatively easy, it is difficult to vary the doping concentration in p-type CdTe because of compensation effects. The most common CdTe thin-film solar cell structure comprises a p-type CdTe absorber layer and n-type CdS window layer forming a hetero-junction, which has an intermixed interface region. Current solar cell structures are based on the device shown in Fig. 10. Different methods for fabricating CdTe films are given in Table 9. Over 10% efficiency was achieved for CdTe cells fabricated by all listed technologies, with the highest to-date efficiency being 16.5% (Wu et al., 2001).

The CdTe solar cells can be grown in both "substrate" and "superstrate" configurations. However, the highest

Table 8
Basic properties of II–VI and I–III–VI_2 films for solar cells.

Properties	II–VI	I–III–VI_2
Absorb. coef., cm^{-1}	10^4–10^5	10^5
Thickness, μm	2–5	2–3
Bandgap, eV	0–3.7 (ZnS)	1.05 (CIS)–3.49($CuAlS_2$)

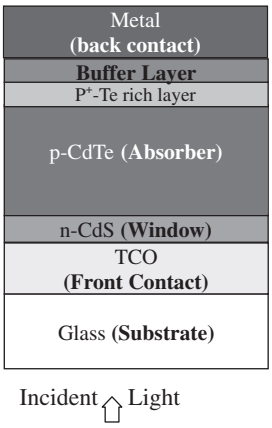

Fig. 10. CdTe/CdS solar cell in "superstrate" configuration.

Table 9
Different methods for fabrication of CdTe films for solar cells.

1. Thermal evaporation	10. Ion-assisted evaporation
2. Electro-deposition	11. Metal–organic chemical vapor deposition
3. Spray pyrolysis	12. Vapor transport deposition
4. Chemical vapor deposition	13. Molecular-beam epitaxy
5. Close-spaced sublimation	14. Atomic layer deposition
6. Chemical molecular-beam deposition	
7. Screen printing	
8. Sputtering	
9. Hot-wall evaporation	

efficiencies have been achieved in "superstrate" configuration. Fig. 10 shows a schematic of a CdTe solar cell grown on a TCO-coated glass substrate in a "superstrate" configuration. The glass substrate can be a low-cost soda-lime glass for a processing temperature below 500 °C, or alkali-free glass (generally borosilicate) for high-temperature processing above 500 °C. A "substrate" configuration would require CdTe to be deposited on metal foils or metal-coated glass substrates. However, the poor quality of the back-contact is a limiting factor in this configuration, because the CdTe/CdS junctions are processed at high temperatures where interdiffusion degrades the CdTe back-contact interface and cells are shunted. Therefore, the "substrate" configuration is not actively pursued in CdTe solar cells.

In the "superstrate" configuration, layers of TCO, CdS, CdTe, and the metal back-contact are sequentially grown on glass substrates. There are some intermediate processing steps that will be described later. An antireflecting coating on the glass rear-surface is often applied to reduce the reflection at the air/glass interface. The incident light passes through the glass, TCO, and CdS, and gets absorbed in the CdTe layer where it creates electron–hole pairs that contribute to the PV power.

5.1.1.1. TCO front electrical contact. A highly transparent and n-type conducting TCO layer with an electron affinity below 4.5 eV is required to form an ohmic contact and to have good band alignment with n-CdS. Most of the TCOs, such as SnO_x:F, ITO, ZnO:Al, and Cd_2SnO_4 (cadmium stannate), have been used to grow high-efficiency (>12%) solar cells. The highest-efficiency (16.5%) cells have been achieved on a bilayer stack of highly resistive Zn_2SnO_4 on a conductive Cd_2SnO_4 by Wu et al. (2001). Although a single layer of TCO produces high-efficiency cells, a bilayer—a combination of high- and low-resistive TCOs as a stack—is often used to protect against shunts caused by pinholes in thin CdS layers. The most commonly used TCO in industrial production is SnO_x:F and often with a thin ITO layer. ITO front contacts are often sensitive to annealing treatment. An increase in electron affinity from around 4–5 eV can be caused by oxidation or post-deposition treatment; moreover, ITO is expensive and should be avoided if possible.

5.1.1.2. CdS window layer. CdS has a bandgap of 2.4 eV and n-type electrical conductivity, forming a heterojunction with the CdTe layer. A typical CdS thickness used in solar cells is in the range of 10–500 nm, under an as-deposited condition. During the high-temperature steps of cell processing, this thickness can be effectively reduced because of interdiffusion with CdTe. A thin CdS layer (10–50 nm) is desired to minimize the photon absorption losses so that the maximum number of photons can reach the CdTe layer. However, there must be a compromise because very thin CdS may lead to a lower open-circuit voltage and fill factor through shunting in the device. CdS layers can be grown by different methods such as chemical-bath deposition (CBD), evaporation, sublimation, vapor transport, metal–organic CVD (MOCVD), and sputtering (McCandless and Sites, 2003; Romeo et al., 1999). Most of the recent progress in these cells has been made by reducing the thickness of the CdS layer.

5.1.1.3. CdTe absorber layer. The CdTe thin film is the most important component as it absorbs the incident solar light and contributes to the photo-generated current. Because of its direct-bandgap, only about 2 μm of material are needed to absorb most of the useful part of the solar spectrum. Another advantage of the CdTe technology is its flexibility with regards to the method of manufacture (Compaan, 2004; Mathew et al., 2003). CdTe layers may be grown by a variety of vacuum and non-vacuum methods, classified into high-temperature and low-temperature processes (Table 9). Some of the commonly used high-temperature methods are close-spaced sublimation (CSS), vapor transport (VT), or vapor transport deposition (VTD), with deposition temperatures above 500 °C. Methods such as electro-deposition (ED), screen printing (SP), chemical spraying (CS), high-vacuum evaporation (HVE), and sputtering with deposition temperatures below 450 °C are classified as low-temperature processes. See the following references for various methods for depositing CdTe layers: CSS (Britt and Ferekides, 1993; Aramoto et al., 1997; Wu et al., 2001), ED (Miyake et al., 2004), sputtering (Gupta and Compaan, 2003), close-spaced VT (Mendoza-Peŕez et al., 2005), spray pyrolysis (Vamsi Krishna and Dutta, 2004), and MOCVD (Hartley et al., 2001; Feng et al., 1996). Depending on deposition methods, the typical thickness of a CdTe layer in solar cells is in the range of 2–6 μm.

One of the critical stages in thin-film solar cell fabrication is the deposition of a CdTe layer with controllable composition and stoichiometry. It has been pointed out that high-efficiency solar cells possess Te-rich CdTe surfaces with smooth interfaces of p-CdTe/n-CdS (Feng et al., 1996). Another issue is fabrication of low-resistivity p-CdTe film, which can be accomplished by incorporating intrinsic point defects and/or by controlling the film stoichiometry; however, this is a complex and difficult issue due to self-compensation. A novel low-cost, non-vacuum chemical molecular-beam deposition method (Razykov,

1991) in atmospheric pressure gas flow allows precise control of the molecular-beam intensities of Cd and Te in the growth process, and can be used to vary the composition and conductivity of CdTe films (Razykov et al., 2009). This method offers advantages over other techniques where controlling film stoichiometry is not possible. The morphologies of CdTe films fabricated by the highest efficiency process – CSS – and the chemical molecular-beam deposition process are shown in Fig. 11a (Razykov et al., 2009) and Fig. 11b (Romeo et al., 2000). The films have very similar morphology.

Despite these problems, remarkable results have achieved over the last few years on thin-film CdS–CdTe solar cells (von Roedern et al., 2005; Compaan, 2004; Schock and Pfisterer, 2001; Razykov et al., 2004). An efficiency of more than 15–16% has been obtained by several researchers (Britt and Ferekides, 1993; Aramoto et al., 1997; Wu et al., 2001). 10.6% and 11.2% efficiencies were obtained on very thin 0.55-μm- and 1-μm-thick CdTe, respectively (Amin et al., 1999). A CdTe cell on plastic foil has an 11.4% efficiency (Upadhyaya et al., 2007). Currently, the cost of a CdTe module is US$ 0.75 fabricated by First Solar (USA).

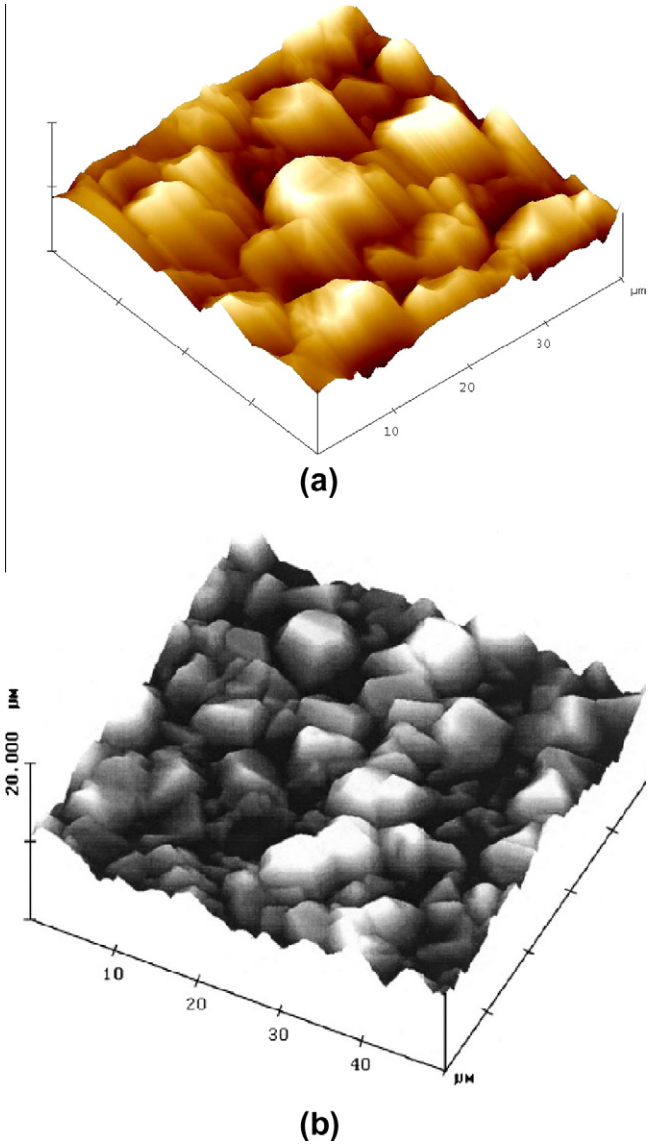

Fig. 11. Morphology (from atomic force microscopy) of CdTe films fabricated by (a) chemical molecular-beam deposition (as deposited), and (b) close-spaced sublimation (on CdS treated in $CdCl_2$).

5.1.1.4. Effect of $CdCl_2$ treatment. The as-deposited CdTe/CdS solar cells always exhibit poor PV properties and thus require a special annealing treatment that improves the cell efficiency considerably (by a factor of 2–3). This is done by subjecting the CdTe/CdS stacks to a heat treatment under Cl-O ambient between 350 and 600 °C. This is known as "$CdCl_2$ treatment" or "junction activation process". After this annealing treatment, a significant enlargement of grain size (depending on the initial grain size) is observed in CdTe grown by low-temperature deposition methods.

For high-temperature growth processes, there is a tendency of CdS_xTe_{1-x} formation by converting small CdS grains into CdTe due to interdiffusion at the interface, and little or low grain growth is noticed after the activation treatment. A stable CdS/CdTe interface can be obtained for a 6% diffusion of sulfur atoms. However, under non-equilibrium conditions, the diffusion of S decreases the thickness of the CdS films, causing pinholes and eventually leading to shorting paths across the junction. This is a critical problem for CdTe solar cells, restricting the application of thinner CdS as desired to minimize the optical absorption losses. Nevertheless, a thermal treatment of the CdS layer prior to CdTe deposition is frequently applied to restrict the interdiffusion of S. The formation of CdS_xTe_{1-x} after activation actually helps in reducing the lattice mismatch between CdS and CdTe—but only marginally, as compared to the improvement in electrical changes induced by Cl, O, and S. Apart from reducing the density of stacking faults and misfit dislocations, there is an overall increase in the shallow-acceptor concentration in CdTe, leading to enhanced p-doping after annealing. In particular, the grain-boundary regions become more p-doped, due to preferred grain-boundary diffusion and segregation of Cl and O. As a result, increased charge-carrier collection efficiency is measured and efficiency increases by a factor of 2–3.

A typical low-temperature photoluminescence (PL) spectrum is shown in Fig. 12 (Razykov et al., 2009a). The peak at 1.41 eV is due to the transition of electrons from the conduction band to the acceptor level $E_v + 0.15$ eV and may be attributed to the vacancy of cadmium V_{Cd}^- or the interstitial atoms of tellurium Te_i^- in CdTe films. The peak at 1.12 eV is possibly caused by a recombination of electrons from a deep donor level E_c – 0.48 eV and free holes in the valence band. This donor level may be attributed to the vacancy of tellurium V_{Te}^{++} or the interstitial atoms of cadmium Cd_i^{++}. After exposure to the $CdCl_2$ heat treatment, the film structure remained essentially unchanged. The PL band located at 1.41 eV

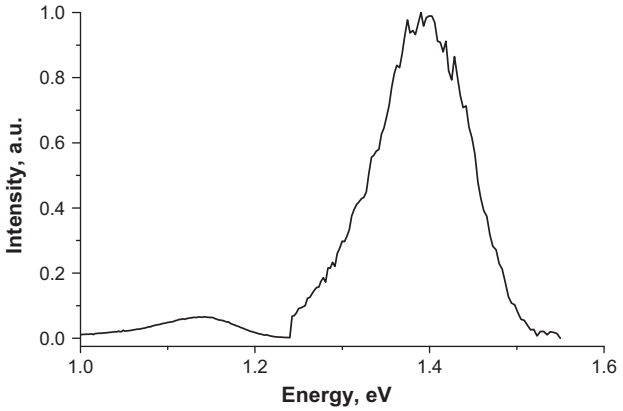

Fig. 12. Photoluminescence spectrum at 20 K for CdTe film with Cd/Te = 1.0.

was still present; however, the 1.12-eV band was annealed out. A tentative conclusion is that the 1.12-eV peak was associated with a tellurium vacancy (V_{Te}^{++}) that was substituted by oxygen following the $CdCl_2$ heat treatment (Razykov et al., 2007). This might be the main reason of the increase in p-CdTe conductivity following the $CdCl_2$ treatment. These results suggest that the $CdCl_2$ heat treatment does not always lead to grain enhancement, in particular for large-grain films; but it does have an effect on the point defects in CdTe films.

5.1.1.5. Problems of electrical back-contact and stability. An important issue in CdTe solar cell technology is the formation of an efficient and stable ohmic contact on the p-CdTe layer. For an ohmic contact to form on a p-type semiconductor, the work function of the metal should be higher that of the semiconductor; otherwise, a Schottky contact is formed. For the p-CdTe layer, a metal with a work function higher than 5.7 eV is. Metals with such high work functions are not available. To overcome this problem, a heavily doped p-CdTe surface is created with the help of chemical etching and a buffer layer of high carrier concentration is often applied. Subsequent post-deposition annealing diffuses some buffer material into CdTe, where it changes the band edges as a result of change in the interface state density. The result is a lowering in interface barrier height and width, which enables a quasi-ohmic or tunnelling contact between the metal and CdTe. Commonly used buffer layer/metallization combinations are Cu/Au, Cu/graphite, or graphite pastes doped with Hg and Cu. But back-contacts containing Cu in any form are often not stable with time because Cu migration from the back-contact leads to efficiency degradation with time. However, alternate processes are being developed; among them, Sb_2Te_3/Mo and Sb/Mo contacts have provided high efficiency and long-term stability (Bätzner et al., 2001, 2004; Romeo et al., 1999; Abken and Bartelt, 2002).

5.1.1.6. Environmental concerns and Cd issue. The CdTe and CIGS thin-film technologies have demonstrated excellent potential for cost-effective production of solar electricity. However, these technologies, especially CdTe, suffer from the perception of toxicity of the constituent element Cd, which is a stable compound in thin-film modules. Issues raised include the hazards associated with the materials used during processing and fabrication of CdTe/CdS and CdS/CIGS solar cells and risks associated during the cradle-to-grave operating lifetime of these modules. The environmental and health hazard issues of CdTe solar modules have been extensively investigated by several independent agencies, including the national laboratories in Europe and USA (Fthenakis et al., 1999). Although CdTe technology has no chance to do away with Cd, there is some maneuverability in CIGS technology in eliminating the very thin (typically ~50 nm) CdS buffer layer; so the quest for an alternative buffer layer is being pursued. Initial success has already been achieved as CIGS solar cells of 16–18.8% and modules of 13.4% have been developed with alternative "Cd-free" buffers (Kushiya, 2004).

Referring to the perception and concerns on Cd issues, Fthenakis (Brookhaven National Laboratory, USA) and Zweibel (NREL, USA) presented a detailed account of their studies at the 2003 National Center for Photovoltaics program review meeting (Fthenakis and Zweibel, 2003) confirming that CdTe panels would be almost benign with zero emission with no associated health hazards. The following points emerged out of their studies:

Cadmium is a by-product of zinc, lead, and copper mining. It constitutes only 0.25% of its main feedstock ZnS (sphalerite). Cadmium is released into the environment from phosphate fertilizers, burning fuels, mining and metal processing operations, cement production, and disposing of metal products. Releases from disposed Cd products, including Ni–Cd batteries, are minimum contributors to human exposure because Cd is encapsulated in the sealed structures. Most human cadmium exposure comes from ingestion and most of that stems from the uptake of cadmium by plants, through fertilizers, sewage sludge, manure, and atmospheric deposition. Although long-term exposure to elemental cadmium, a carcinogen, has detrimental effects on kidneys and bones, limited data exist in toxicology. However, the CdTe compound is more stable and less soluble than elemental Cd, and therefore, likely to be much less toxic.

There is a gaseous emission of 0.001% Cd during the electrolytic refinery production of CdTe powders (from Cd wastes from Zn, iron, and steel industries). This would correspond to 0.01 g/GW h, which is significantly less than 0.5 g/GW h. The only potential hazard that could come to mind would be a building fire. It has also been estimated quantitatively that the maximum temperature of a basement on fire is ~900 °C, which is still less than the melting point of CdTe (1041 °C). Besides, the vapor pressure at 800 °C for CdTe is ~2.5 torr (0.003 atmosphere), so this minimizes the risks further, and once sealed between glass plates any Cd vapor emission is unlikely. The main conclusion of the studies was that the environmental risks

associated with CdTe-based technology are minimal. Every energy source or product may present some direct or indirect environmental health and safety hazards, but those of CdTe should by no means be considered a problem. The following conclusions were drawn:

- Cd is produced as a by-product of Zn and can either be put to beneficial uses or discharged to the environment, posing health risks.
- CdTe in PV is much safer than other current Cd uses.
- CdTe PV uses Cd 2500 times more efficiently than Ni–Cd batteries.
- Occupational health risks are well managed.
- During PV operations, there as absolutely no emissions.
- A risk from fire emission is minimal.
- CdTe technology and modules are safe and do not pose significant risks.

5.2. I–III–VI_2 solar cells

Among I–III–VI_2 compounds, $CuInSe_2$ has very attractive properties for thin-film solar cells (Table 8): (a) a very high optical absorption coefficient ($\approx 10^5$ cm^{-1}) and consequently, a very thin layer (0.1–0.3 μm) is suitable for solar cells; (b) the possibility to change the type of conductivity (p-or n-) and resistivity; (c) the formation of solid solutions (different bandgaps), allowing bandgap engineering and therefore the fabrication of high-efficiency thin-film solar cells.

Its bandgap of l eV is rather low for solar cells, and it is usual to replace indium with an alloy of indium and gallium—Cu(In,Ga)Se_2—to increase the bandgap and hence the open-circuit voltage. Different methods for fabricating these films are given in Table 10. The best results have been obtained on cells fabricated by co-evaporation. The world-record efficiency of almost 20% (the highest value for thin-film cells) on a CIGS cell was achieved at NREL (Ramanathan et al., 2003; Repins et al., 2008). A CIGS cell on metal foil attained a 17.5% efficiency (Upadhyaya et al., 2007). In terms of large-scale terrestrial applications, this material has a disadvantage because indium and gallium are very limited resources. Recently, aluminium was used instead of gallium, and more than 17% efficiency was obtained for Cu(In,Al)Se_2 cell (Marsillae et al., 2002). It should be noted that the passivation process (a key step for a-Si and pc-Si technologies) is not necessary for II–VI and I–III–VI_2 thin-film solar cells. This can be due to the effect of "self-passivation" suggested by Razykov (1996) (Fig. 13). Remarkable results have been achieved on polymer substrates (Upadhyaya et al., 2007).

Table 10
Different methods for fabrication of Cu(In,Ga)Se_2 films.

1. Co-evaporation	6. Hybrid evapor./sputtering
2. Electrodeposition/sele-nization	7. Reactive sputtering
3. Electron beam/selenization	8. Spraying
4. Hybrid selenization	9. Close-spaced vapor transport
5. Sputtering selenization	

5.2.1. Material and properties

Compound semiconductors from the I–III–VI_2 series of the periodic table, such as copper–indium–diselenide (CIS), copper–gallium–diselenide (CGS), and their mixed alloys copper–indium–gallium–selenide (CIGS), are often simply referred to as chalcopyrites because of their tetragonal crystal structure. These materials are easily prepared in a wide range of compositions, and their corresponding phase diagrams have been intensively investigated. Changing the stoichiometry and extrinsic doping can vary their electrical conductivity. However, in preparing solar cells, only slightly Cu-deficient compositions of p-type conductivity are suitable. Depending on the [Ga]/[In + Ga] ratio, the bandgap of CIGS can be varied continuously between 1.04 and 1.68 eV. The current high-efficiency devices are prepared with a bandgap in the range 1.20–1.25 eV; this corresponds to a [Ga]/[In + Ga] ratio between 20% and 30%. Layers with higher Ga content, as needed to increase the bandgap toward ~1.5 eV, are of inferior electronic quality and yield lower-efficiency cells.

Other chalcopyrites, such as $CuInS_2$ and $CuInTe_2$, were also investigated earlier, but cell efficiencies were rather low and the R&D focused on CIS. Recently, interest in $CuInS_2$ has resurfaced with the development of ~11.4%-efficient cells at HMI Berlin. A spin-off company Sulfurcell, based in Berlin, started setting up a pilot production line in 2003. The device structure of the $CuInS_2$ solar cell is quite similar to CIGS solar cells in terms of other constituent layers.

The first CIS solar cell developed with single-crystal material and ~12% efficiency was reported by Wagner et al. (1974). The first thin-film solar cell was reported by Kazmerski et al. (1976) by developing ~4%-efficient cells obtained by the evaporation of $CuInSe_2$ material (Kazmerski et al., 1976). The real breakthrough in CIS

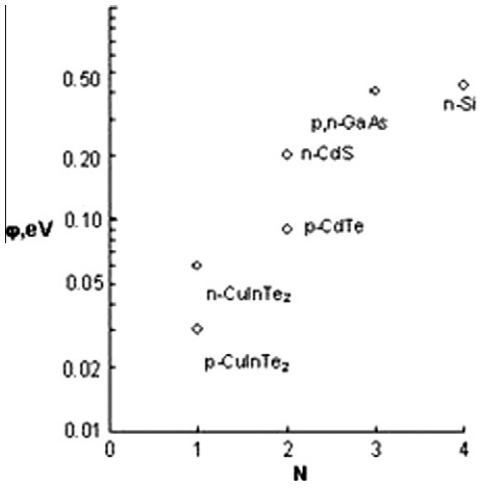

Fig. 13. Dependence of the intergrain energy barrier height on the valency of low-valent element of different polycrystalline semiconductors.

thin-film technology came with the pioneering work of Boeing Corporation (USA), where they used three-source evaporation of Cu, In, and Se elements and raised the efficiency from 5.7% in 1980 to above 10% in 1982. This success, despite the apparent complexity of the material system, clearly showed the promising potential of this material. Later, in 1987, Arco Solar (USA) raised the cell efficiency to ~14% by using a different CIS deposition process where a stacked metal layer was selenized under H_2Se ambient. Subsequent improvements in efficiency were attained by the EUROCIS consortium in Europe and later at NREL (USA), who hold the efficiency record of ~19.5%, which is highest for any thin-film, single-junction solar cell (Ramanathan et al., 2003). Efficiency improvements over the Boeing process occurred due to adding Ga and S for bandgap engineering, adding Na in the absorber layer, and optimising the n-CdS (hetero-junction part of the cell) and transparent front electrical contact layers.

The first industrial production of CIS modules was started by Siemens (later Shell Solar) based on the Arco Solar technology. Other industries such as Wurth Solar and Global Solar started developing CIS solar modules with co-evaporation methods. Several other companies have been investigating various other methods of deposition such as paste printing and electro-deposition, but up to now, these technologies have been less successful compared to vacuum-based technologies.

The phase diagram of the ternary compound is described by a pseudo-binary phase diagram of the binary analog, e.g., Cu_2Se and In_2Se_3 phase for $CuInSe_2$ ternary. Single-phase chalcopyrite $CuInSe_2$ exists at a small copper deficiency. For Cu-rich compositions, a mixed phase of Cu_xSe with $CuInSe_2$ forms, which is not suitable for PV devices. Despite a complicated crystal structure and multi-component system, the material properties of the PV-relevant compounds are fault-tolerant and not much affected by minor deviations from stoichiometry in the Cu-deficient range. Also, surfaces and grain boundaries in CIGS compounds are easy to passivate, resulting in high-efficiency cells even with sub-micron grain-size materials.

The PV-grade Cu-deficient CIGS material has a tetragonal crystal structure with vacancies and interstitials that act favorably, especially because the material is self-healing due to defect relaxation caused by highly mobile Cu ions and its interaction with vacancies. Defects created in CIGS by external influence (e.g., radiation) are immediately healed. This is an inherent advantage of the CIGS material, leading to highly stable CIGS solar cells. However, care must be taken for proper encapsulation of devices against very damp conditions; otherwise, the degradation of the electrical contact (TCO or Mo) in moisture can lead to minor degradations. Therefore, stability of encapsulated CIGS solar cells is not a problem as proven by field tests conducted by ZSW, Shell, and NREL. CIGS is also tolerant against space radiation, being superior to Si and GaAs single-crystal cells, but somewhat inferior to CdTe.

5.2.2. CIGS solar cell configuration

CIGS solar cells can be grown in both "substrate" and "superstrate" configuration, but the substrate configuration gives the highest efficiency due to favorable process conditions (Fig. 14). However, it requires an additional encapsulation layer and or glass to protect the cell surface, which is not required in the superstrate configuration. Superstrate structures were investigated in the early 1980s, but their efficiency was less than 5%. However, recent efforts have improved the efficiency up to ~13%. This has been possible with the introduction of undoped ZnO instead of a CdS buffer layer and co-evaporation of Na_xSe during the CIGS deposition. Further, developments in bifacial CIGS solar cells, with both front and rear transparent conducting contacts, are making significant progress (Nakada et al., 2004).

5.2.2.1. Electrical back-contact. CIGS solar cells in substrate configuration can be grown on glass, as well as on metal and polymer foils. Molybdenum, grown by sputtering or e-beam evaporation, is the most commonly used electrical back-contact material for CIGS solar cells. Growth of the solar cell starts with the deposition of Mo on the substrate, which forms an electrically conducting back-electrode with CIGS. When CIGS is grown on Mo, an interface layer of $MoSe_2$ is automatically formed that helps in ohmic transport between CIGS and Mo. Recently,

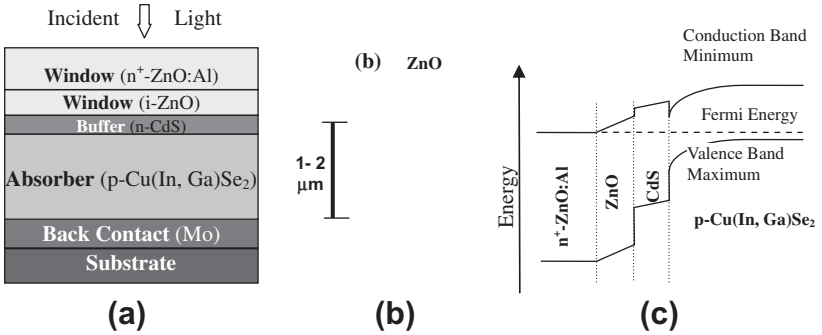

Fig. 14. (a) CIGS solar cell in "substrate" configuration, (b) SEM cross-section image of CIGS device showing microstructure of layers, and (c) qualitative energy band diagram of CIGS solar cell.

alternative back-contact materials have been explored, but industrial production is still based on Mo layers.

5.2.2.2. CIGS absorber layer. Because of a high absorption coefficient, a 2-μm-thick layer is sufficient for absorption of maximum incident radiation. CIGS layers can be grown with a variety of deposition methods. Although the grain size and morphology (surface roughness) depend on the deposition method, high efficiencies exceeding 13% have been achieved with most of the methods, which indicates that grain boundaries in CIGS are benign and can be easily passivated. High-efficiency cells have p-type $Cu(In,Ga)Se_2$ bulk, whereas a defect-chalcopyrite $Cu(In.Ga)_3Se_5$ phase, in the form of a thin layer that segregates at the top surface, is n-type especially when doped by cation atoms diffusing from the buffer layer. It is believed that this inverted surface, leading to a p–n homojunction in the CIGS absorber, is crucial for high-efficiency cells.

5.2.2.3. Buffer layer. Several semiconductor compounds with n-type conductivity and bandgaps between 2.0 and 3.4 eV have been applied as a buffer to form a hetero-junction in CIGS solar cells. However, CdS remains the most widely investigated buffer layer, because it has continuously yielded high-efficiency cells. CdS for high-efficiency CIGS cells is commonly grown by CBD, which is a low-cost, large-area process. However, incompatibility with in-line, vacuum-based production methods is a concern. Physical vapor deposition (PVD)-grown CdS layers yield lower-efficiency cells, because thin layers grown by PVD do not show uniform coverage of CIGS and are less effective in chemically engineering the interface properties between the buffer and absorber. The recent trend in buffer layers is to substitute CdS with "Cd-free" wide-bandgap semiconductors and to replace CBD with in-line-compatible processes. Alternative materials such as In_2S_3, ZnO, ZnS, and ZnSe using different methods such as PVD, radio-frequency (RF) sputtering, MOCVD, atomic layer deposition (ALD), or a novel technique called ion layer gas reaction (ILGAR) are being explored (Chaisitsak et al., 2001; Ohtake et al., 1995; Bhattacharya and Ramanathan, 2004; Spiering et al., 2003). A record efficiency of 18.8% has been achieved for CBD-ZnS recently (Nakada and Mizutani, 2002). Most industries are currently using CBD-CdS, but Showa Shell has shown 14.2% efficiency for an 864-cm^2 submodule developed with CBD-grown ZnS(O,OH) buffer layers (Kushiya, 2004).

5.2.2.4. Front electrical contact. TCOs with bandgaps above 3 eV are the most appropriate and have become the ultimate choice for front electrical contacts due to their excellent optical transparency (>85%) and reasonably good electrical conductivity (Wang et al., 2009). Today, CIGS solar cells use either ITO or, more frequently, RF-sputtered Al-doped ZnO. A combination of an intrinsic and a doped ZnO layer is commonly used, and although this double layer yields consistently higher efficiencies, the beneficial effect of intrinsic ZnO is still under discussion. Doping of the conducting ZnO layer is achieved by group III elements, particularly aluminium. However investigations show boron to be a feasible alternative because it yields a high mobility of charge carriers and a higher transmission in the long-wavelength spectral region, giving rise to higher currents. For high-efficiency cells, the TCO deposition temperature should be lower than 150 °C to avoid the detrimental interdiffusion across the CdS/CIGS interface. RF sputtering is not considered suitable for industrial production; therefore, alternative sputtering and CVD methods are investigated and used.

5.2.2.5. Sodium incorporation in CIGS. One of the breakthroughs in CIGS PV technology occurred when the alumina or borosilicate glass substrate was replaced by soda-lime glass to match the thermal expansion coefficients, resulting in substantial improved efficiency. Subsequently, sodium was realized to play an important role (Hedström et al., 1993) in high-efficiency CIGS solar cells because it affects the microstructure (grain size) and passivates the grain boundaries, leading to changes in electronic conductivity by up to two orders of magnitude. The overall effect is efficiency improvement primarily because of an increase in the V_{oc} and FF of the solar cells. Most commonly, Na is introduced into CIGS by diffusion from the soda-lime glass substrate during absorber deposition. However, Na incorporation from such an approach is neither controllable nor reliable; therefore, alternative methods to add Na from external sources are used either during or after the deposition of CIGS layers. These methods include the co-evaporation or the deposition of a thin precursor of a Na compound such as NaF, Na_2Se, or Na_2S for CIGS on Na- free substrates, which include soda-lime glass covered with barrier layers (e.g., Al_2O_3, Si_3N_4, as used by Shell Solar). These barrier layers inhibit sodium diffusion from the glass substrate. CIGS on flexible substrates (metal and polymide foils) also need controlled incorporation of sodium, which is provided from a precursor layer applied prior to or after the CIGS growth.

5.2.2.6. Deposition and growth of CIGS absorber. There are several processes for depositing CIGS thin films, some of which are briefly described below.

5.2.2.6.1. Co-evaporation processes. As described earlier, vacuum evaporation is the most successful technique for depositing CIGS absorber layers for highest-efficiency cells. The vacuum evaporation method involves simultaneous evaporation of the constituent elements from multiple sources in single or sequential processes during the whole absorber deposition process. A variation of the In-to-Ga ratio during the deposition process leads to only minor changes in the growth kinetics; however, the variation of the Cu content strongly affects film growth. Thus, different co-evaporation growth procedures are classified by their Cu evaporation profile (Fig. 15).

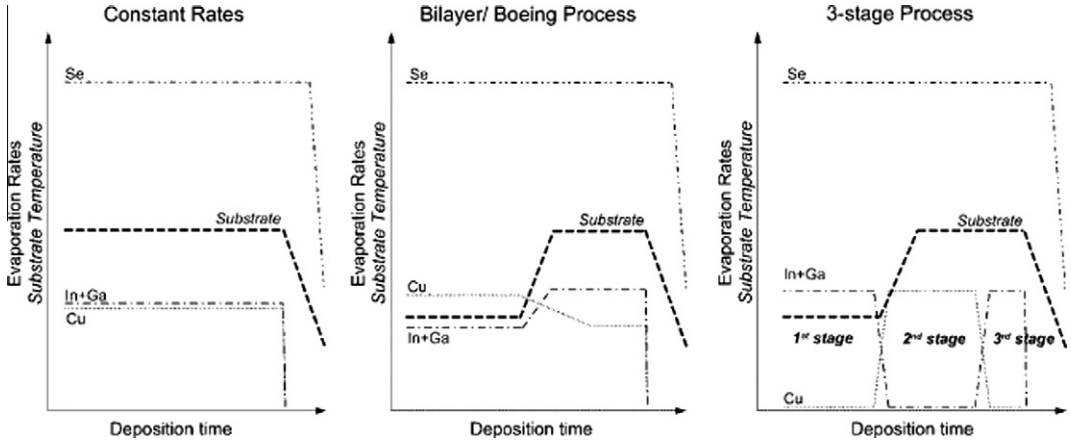

Fig. 15. Diagram representing the recipes in the co-evaporation processing steps in the deposition of $Cu(In,Ga)Se_2$ used for constant rate, bilayer (Boeing), and three-stage processes.

One variant of co-evaporation is a bilayer process (the "Boeing process"), which originates from the work of Mickelsen and Chen (McCandless and Dobson, 2004) and yields larger grain sizes compared to the constant-rate (single-stage) process. This result is attributed to the formation of a Cu_xSe phase during the Cu-rich first stage that improves the mobility of group III atoms during growth.

The highest laboratory efficiencies are achieved with the so-called "three-stage" process, introduced by NREL (Gabor et al., 1994). With this process, the CIGS layer is obtained by starting the deposition of an $(In,Ga)_xSe_y$ precursor, followed by the co-deposition of Cu and Se until a Cu-rich overall composition is reached; finally, the overall Cu concentration is readjusted by subsequent deposition of In, Ga, and Se. CIGS films prepared by the three-stage process exhibit a large-grained smooth surface, which reduces the junction area and is thereby expected to reduce the number of defects at the junction and yield high efficiency. Several groups worldwide have developed 16–19.5%-efficiency cells using CIGS grown with the three-stage process.

5.2.2.6.2. Selenization of precursor materials. This sequential process is favorable due to its suitability for large-area film deposition with good control of the composition and film thickness, shown by the initial success of Arco Solar in 1987. Such processes consist of the deposition of a precursor material obtained by sputtering, evaporation, electro-deposition, paste printing, or spray pyrolysis, followed by thermal annealing in a controlled reactive or inert atmosphere for optimum compound formation via the chalcogenization reaction (Fig. 16). The precursor materials are either stacked metal layers or a stack of their compound and alloys. Shell Solar (USA) and Showa Shell (Japan) use the sputtering technique for precursor deposition and production of large-area solar modules up to 60 cm × 120 cm, yielding maximum efficiencies of 13% on 30 cm × 30 cm modules (Karg, 2001; Kushiya et al., 2003; Palm et al., 2004). Solar modules produced by Shell Solar are commercially available in the market.

5.2.2.6.3. Alternative CIGS growth processes. There is substantial interest in using non-vacuum methods for CIGS deposition. An innovative approach uses the stability of the oxides to produce nano-sized precursor particles (Kaelin et al., 2004; Eberspacher et al., 2001). Nano-sized metal oxides are mixed in an ink suspension, which allows low-cost, large-area deposition by doctor blading, screen printing, or spraying of the precursor. Such non-vacuum deposition of precursors allows a very efficient material utilization of almost 100% of the non-abundant indium and gallium metals. A selenization treatment converts the precursor into a CIGS layer, resulting in solar cell efficiencies of over 13% as reported by ISET (USA). One of the drawbacks of the process is the toxicity of the H_2Se gas used for selenization. However, recent efforts are focusing on selenizing printed precursors with Se vapors (Kaelin et al., 2004).

The CIGS compound can also be formed directly by electro-deposition from a chemical bath. Several groups, including EDF-CNRS (France), CIS Solar Technologies (Germany), and CISCuT (Germany), have been using such approaches and obtained >10%-efficient cells. With a hybrid approach using additional vacuum deposition on an electrodeposited precursor layer, NREL (USA) has achieved efficiencies as high as 15.4%.

5.2.2.7. Flexible CIGS solar cells. The ultimate advantage of thin-film technology is roll-to-roll manufacturing to produce monolithically interconnected solar modules leading to low time for energy payback because of high-throughput processing and to low cost of the overall system. A large number of activities on highly efficient, stable, and flexible thin-film modules based on CIGS has recently drawn much interest for flexible solar cells on metal and plastic foils. Apart from the expected high efficiency and long-term stability for terrestrial applications, flexible CIGS has excellent potential for space application because of their tolerance to space radiation, being 2–4 times superior to conventional Si and GaAs cells. Lightweight and rollable solar array structures will reduce the overall cost of

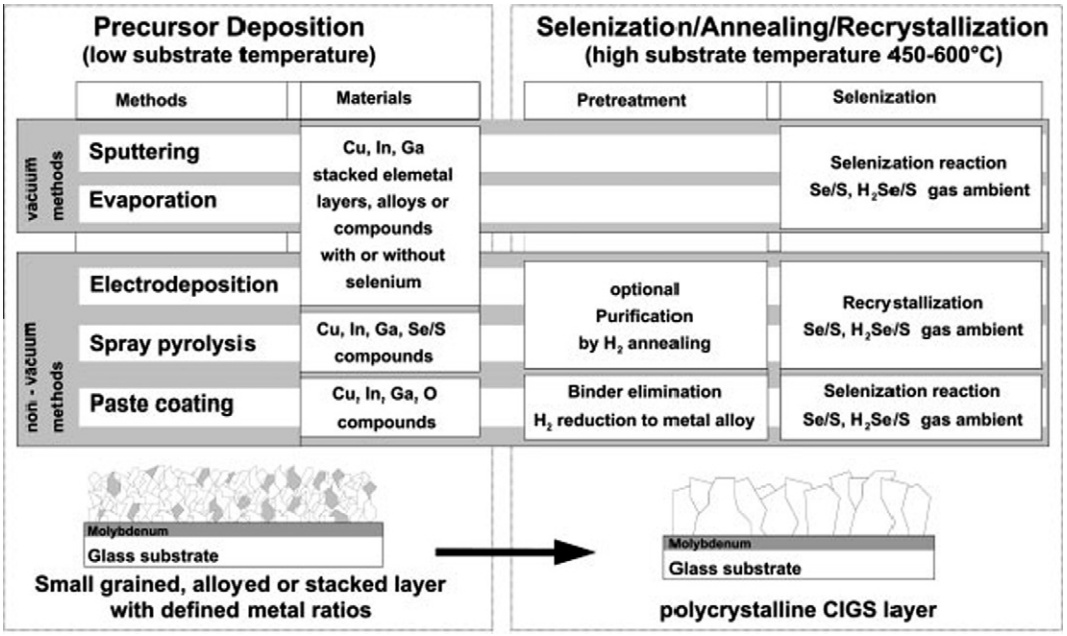

Fig. 16. Various processes for selenization of precursor materials for CIGS cells.

space-deployable solar modules, but can also substantially save on the cost of launching satellites.

Development and current status of flexible CIGS solar cells have been reviewed by Kessler and Rudmann (2004). Flexible CIGS cells can be grown on polymide and on a variety of metals, e.g., stainless steel, Mo, and Ti. Therefore, the choice of substrate is important due to some advantages and disadvantages: (i) The density of usable metals is 4–8 times higher than polymer; therefore, cells on metals are heavier; (ii) metals are conducting and have rough surfaces; therefore, monolithic module development is difficult, which, in contrast, is easier on polymer foils; (iii) stainless-steel foils need an extra barrier layer against detrimental impurity (e.g., Fe) diffusion of the metal into the CIGS during deposition; and (iv) metal foils can withstand high deposition temperatures (550–600 °C); this leads to higher efficiency than on polymer foils, which are not suitable for processing temperatures >450 °C.

High record efficiencies of flexible CIGS solar cells are 17.5% on stainless steel by Daystar (USA) and 14.1% on polymer foil by ETH (Zurich, Switzerland). Several research groups and industries are involved in developing flexible solar cells, but Global Solar (USA) is the only company manufacturing flexible CIGS on a pilot production line. They have reported a 13.17% cell (68.8 cm^2) and modules of 11.13% (3898 cm^2) and 10.10% (7085 cm^2) efficiencies on metal foils. The solar modules on stainless-steel foil are not monolithically connected, but they are made by individually connecting large-area cells with an overlap method. ZSW (Germany) is developing a scribing and patterning method for monolithically connected solar modules on metal and polymer foils. The basic schematic cross-section of a monolithic module on glass is shown in Fig. 17, along with a flexible prototype mini-module developed on polymer foil by ZSW and ETH (Zurich) within a European collaborative project.

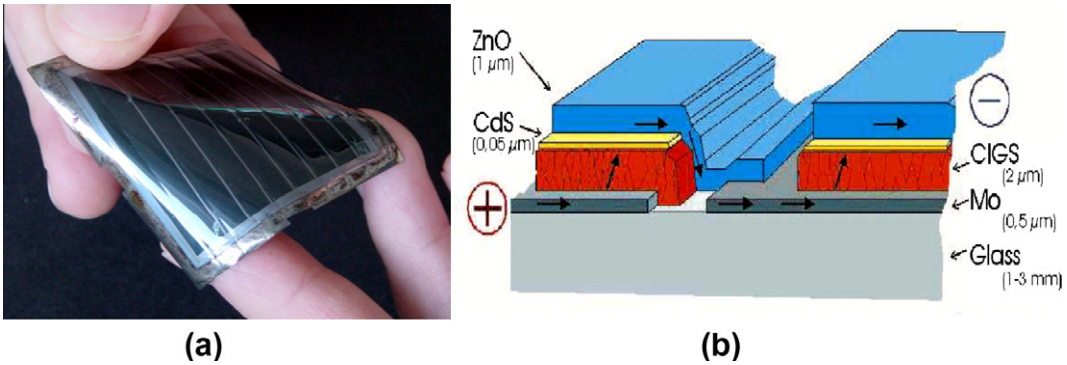

Fig. 17. (a) Flexible monolithic CIGS modules showing a prototype mini-module on a polymer foil, and (b) schematic cross-section of the module exhibiting the material component layers and their interconnect patterns.

Table 11 gives an overview of different flexible solar cell technologies, including the organic and TiO_2 dye-sensitized PV technologies. Because of the late start in R&D on flexible CIGS and CdTe solar cells, they are industrially less mature compared to a-Si cells. However, high cell efficiency and inherent stability advantages indicate a promising potential for these technologies. The best thin-film CIGS module efficiency is 11.0% (Table 12).

For most of the leading technologies, efficiency is already adequate (Table 13), and emphasis should be on developing cost-effective manufacturing technologies that can significantly lower the production cost below US$ 1.5/W_p. The production cost of thin-film CdTe solar module is US$ 0.76/W_p (First Solar). The selling price of CdTe and CIGS and a-Si are US$ 2.0–2.25/W_p (Table 13) (von Roedern, 2010). These values can be significantly reduced with high production volume.

6. III–V single- and multi-junction solar cells

The theoretical efficiency of a single-junction cell is around 31%. Better efficiencies could be obtained with more-efficient use of the solar spectrum. Combining two or more cells of different bandgaps into a multi-junction arrangement increases the amount of work done per photon. To increase power, the cells should be current matched and joined in series—separated, for example, by a tunnel diode. An obvious way to increase the efficiency is to construct tandem cells having a larger number of materials with different bandgaps The best multi-junction cells have already reached an efficiency around 41%; however, the technology is very expensive and these solar cells are therefore used today mainly for space applications.

In terms of space power applications, the Si cell efficiency is low and susceptible to radiation damage. In the late 1980s, GaAs cells were used to fabricate flat-plate arrays due to high efficiencies and lower radiation-induced degradation than Si cells. GaAs single-junction solar cells with efficiencies of ~25% were reported for concentrated AM0 sunlight many years ago (Sundaram et al., 1992; Andreev, 1994). MOCVD, liquid-phase epitaxy, and molecular-beam epitaxy (MBE) are usual methods for fabricating III–V solar cells.

Enhanced efficiencies may be realized by stacking GaAs either monolithically or mechanically on booster cells of lower-bandgap materials such as Si, Ge, CIS, GaSb, or InGaAs. For ultra-high-efficiency cells to be widely applied, it will be necessary to improve conversion efficiency and reduce cost. One approach is the fabrication of GaAs/Si cells. However, in this case, GaAs films contain dislocations. Another problem is that impurity diffusion from highly doped tunnel junctions during overgrowth of the top cell increases the resistivity of the tunnel junction.

The InGaP/InGaAs/Ge triple-junction concentrator solar cell has demonstrated ~37.0% efficiency (Yamaguchi et al., 2005). The concentration ratio is defined by the increase in I_{sc} and I_{sc}/I_{sc}(1-sun) ratio. High conversion efficiency of more than 36% is measured under concentrated light with a concentration ratio ranging from 30 suns to 200 suns of AM1.5G. At a concentration ratio of 200 suns of AM1.5G, the conversion efficiency was measured at 37.4%. New approaches on novel materials and structures for 50%-efficient multi-junction cells are presented by Yamaguchi et al. (2008).

7. Nanophotovoltaics

The superior optical, electric, and chemical properties of nanomaterials offer the chance for solar cells to get higher efficiencies. At present, three competing types of nanotechnology are being applied to solar cell development, each classified by material: crystalline semiconductor III–V materials, polymeric materials, and carbon-based nanostructures. Each has different potential applications and different ways of attempting to overcome the cost/efficiency trade-off.

7.1. Quantum well solar cells

Competitive costs and performance can be achieved by using quantum wells and quantum dots in crystalline solar cells. The quantum well solar cell (QWSC) is a novel device with the potential to achieve high efficiency in an alternative approach to tandem or cascade solar cells. QWSCs were reviewed by Barnham et al. (2003). Different losses in a standard p–n-junction limit the efficiency to ~30%,

Table 11
Overview of different flexible solar cell technologies.

	CIGS	CdTe	Amorphous silicon	Organic and titanium oxide
Lab efficiency on plastic foil	14.1% (single-junction cell)	11.4% (single-junction cell)	8%*–12%* (multi-junction cell)	5–8%
Lab efficiency on metal foil	17.5% (single-junction cell)	8% (single-junction cell)	14.6%*/13% (multi-junction cell)	
Industrial efficiency (typical values)	6–11% (On steel foil, not yet available on plastic foil)	Not yet demonstrated	4–8%* (available on plastic and metal foils	Not yet demonstrated
Stability under light	Material stable	Material stable	Degrades	Stability not proven

[a] Initial values measured before light-induced degradation of solar cells.

Table 12
Best production-line PV module efficiency values from manufacturers' websites compiled by Bolko von Roedern September 2009.

Ranked module efficiency (%)	Description of best module	Same module with lowest power rating
19.3 (non-stan)	**SunPower** 315 (SunPower rear-point contacted cells, mono-Si) Tcoeff. = −0.38%/C, V_{oc}/cell = 673 mV	Also SunPower 305, efficiency 18.7%
17.1 (non-stan)	**Sanyo** HIP-215NKHAS (single crystal CZ Si, HIT (Tcoeff. = −0.30%/C), V_{oc}/cell = 717 mV	Also HIP-200, efficiency 15.9% (warranty is 10/86 + 20/76)
14.4 (multi)	**Suntech Stp280-24/Vd** (multi-Si) Tcoeff. = −0.47%/C, V_{oc}/cell = 622 mV	Also Suntech STP260, efficiency then 13.4% (warrant 10/90 + 25/80)
14.4 (mono)	**BP** 4180T, Tcoeff. = −(0.5 ± 0.05)%/C, V_{oc}/cell 606 mV	Also BP4165, efficiency then 13.1%
14.1 (multi)	**Kyocera** KD210GX-LP (cast multi-Si diffused cells) Tcoeff. (only given for V_{oc}, −0.123 V/C), V_{oc}/cell = 609 mV	Also as 205 W, eff then 13.8%
14.1 (mono)	**Suntech STP180S-24/Ad** (mono-Si) Tcoeff. = −0.48%/C, V_{oc}/cell = 622 mV	Also STP170, efficiency then 13.3% (10/90 + 25/80)
14.1 (mono)	**Sharp** U-175 (mono-Si, standard) −0.485%/C, V_{oc}/cell = 617 mV	Also Sharp NU-170, efficiency 13.0%
13.8 (multi)	**BP** 3230 N multi-Si standard cells) Tcoeff. = −(0.5 ± 0.05)%/C, V_{oc}/cell = 607 mV	Also 220 W, efficiency 13.2%, warranty is 12/90 + 25/80
13.7 (mono)	**SolarWorld Sunmodule 230/220** (mono-Si "Shell") Tcoeff.: V_{oc} = −0.33 V/C, V_{oc}/cell = 617 mV	Also220 W, efficiency 13.1% Power warranty 12/90%, 25/80%
13.7 (multi)	**Sharp** ND-224-UC1 (multi-Si, diffused) Tcoeff. = −0.485%/C, V_{oc}/cell = 610 mV	Also as Sharp 216, then 13.3% efficient, 25/76 warranty
13.4 (ribbon)	**Evergreen Solar** ES 210 (string ribbon Si) Tcoeff. = −0.45%/C	Also ES-200 efficiency 12.7%
11.0 (CIS)	**WürthSolar** WS GOO25 E080 (CIS) Tcoeff. = −0.36%/C	Also WS GOO25 E075, efficiency 10.3% (warranty 20/80%)
10.8 (CdTe)	**First Solar** FS-277 (CdTe) Tcoeff. = −0.25%/C (above 40 C −0.2%/C below 40 C, V_{oc}/cell = 773 mV	Also FS-270, efficiency 9.7% (25-y ltd warranty)
9.0 (a-Si/nc-Si)	**Sharp** NA-V128H5 (128-W) (amorphous/nanocrystalline Si tandem) Tcoeff. = −0.24%/C	Also Sharp NA-V115H5 (115 W) Efficiency 8.1% (warranty: 10/81, 25/72)
8.4% (a-Si/nc-Si)	**Sunfilm** Q120 (amorphous/nanocrystalline Si tandem) Tcoeff. = −0.3%/C	Also Q110, then eff. is 7.7%
8.3 (a-Si/nc-Si)	**Mitsubishi Heavy** MT 130 (a-Si/nc-Si tandem, VHF deposition), Tcoeff. = −0.28%/C	Only one rating
7.6 (CdTe)	**Calyxo CX 55** (CdTe) Tcoeff. = −0.25%/C	Also as 40 W, then eff. is 5.6%
6.7 (a-Si 3-j)	**Uni-Solar** PVL 144 (triple-j. amorphous silicon roofing laminate), Tcoeff. = −0.21%/C	Also as 124 W, eff. 5.7% (20/80 warranty)
6.3 (a-Si 1-j)	**Kaneka** T-SC(EC)-120 (single-j. a-Si) No Tcoeff. given	Only one rating (ltd warranty 25/80%)
6.2 (a-Si 1-j)	**Bosch Solar** T 90 (single-j. a-Si) Tcoeff. = −0.21%/C	Also available as 75 W, eff. then 5.3%
6.0 (a-Si/a-Si)	**EPV** 5 × 56 W (same-bandgap double-junction a-Si) Tcoeff. = −0.19%/C	Also 50 W, eff 5.3% (warranty is 25/80)
1.7 (organic)	**Konarka** KT 3000 (26 W) Tcoeff. −0.27%/C (based on temperature)	No power warranty, only one rating

and ways to avoid these losses to significantly increase the efficiency of QWSCs are analysed by Green (2000a,b). In the simple QWSC, quantum wells of a lower-bandgap material are grown within the space-charge region of p–n or p–i–n-structures. MBE or MOCVD are used to fabricate QWSCs.

Incorporating CdTe quantum wells into $Cd_xMn_{1-x}Te$ p–i–n structures has been shown to successfully extend the photoresponse to longer wavelengths (Ashenford et al., 1995). The QWSC can enhance the short-circuit current and open-circuit voltage (V_{oc} = 1.07 V for QWSC and 1.022 V for the usual cell) over a comparable conventional cell formed from the barrier material. An AlGaAs/GaAs QWSC also enhances efficiency over comparable AlGaAs cells becasue of reducing recombination losses (Barnham et al., 2003; Ekins-Daukes et al., 2000). The current status of QWSCs was recently described by Mazzer et al. (2006).

7.2. Quantum dot solar cells

Quantum dots (QDs) are nanometer-sized crystallite semiconductors that can be produced by a variety of methods (Woggan, 1997). The advantage of QDs is the ability to tune the absorption threshold simply by choosing the dot diameter. Theoretical results of Luque and Marti (1997) have shown that solar cells with an intermediate band of states resulting from the introduction of QDs can exceed the Shockley–Queisser model efficiency of not only a single junction, but also, of a tandem cell. A QD is a granule of a semiconductor material on the nanometer scale, and these nanocrystallites behave essentially as a three-dimensional potential well for electrons (i.e., the quantum mechanical "particle in a box"). By introducing a single-sized dot into an ordered array within the intrinsic region of a p–i–n solar cell, Luque and Marti calculated a theoretical efficiency of 63%.

Table 13
Commercial thin-film modules, data taken from websites (compiled by Bolko von Roedern (NREL); 09/2010).

Module eff. (%)	Description	Output (W)	Selling price ($/$W_p$)
12.0	**Q-Cells (Solibro)** UF-90 (CIS) Tcoeff. = −(0.38 ± 0.04)%/C	Also UF-70, eff. then 9.3% W: 10/90, 25/80	~$ 2.25/W
11.9	**AVANCIS** 130 W (CIGS), Tcoeff. = −0.45%/C	Also 100 W, eff. then 9.2%, 20 y ltd w	~$ 2.25/W
11.0	**WürthSolar** WS GOO36E080 (CIGS) Tcoeff. = −0.36%/C	Also WS GOO36E070, efficiency 10.3% (warranty 20/80%)	~ $ 2.25/W
11.1	**First Solar** FS-380 (CdTe) Tcoeff. = −0.25%/C (above 40 C, −0.2%/C below 40 C	Also FS-370, efficiency 9.7% (warranty: 10/90, 25/80)	~$ 2.25/W
10.7	**Solar Frontier SF85-US-B** (CIGS) Tcoeff. = −0.35%/C	Also 80 W, eff. then 10.1% (w: "competitive")	~$ 2.25/W
9.0	**Calyxo CX 55/65** (CdTe) Tcoeff. = −0.25%/C	Also as 55 W, then eff. is 7.6%	~$ 2.25/W
6.7	**Uni-Solar** PVL 144 (triple-j. amorphous silicon roofing laminate), Tcoeff. = −0.21%/C	Also as 136 W, eff. 6.3% (25/80 warranty)	~$ 2.25/W
6.3	**Kaneka** T-SC(EC)-120 (single-j. a-Si) No Tcoeff. Given (link requires Jap. language font)	Only one rating (ltd warranty 25/80%)	~$ 2.00/W
1.7	**Konarka** 620 (7.7 W) Tcoeff. + 0.05%/C (based on air-T), (organic)	No power warranty, only one rating	N.A.

Quantum dots are commonly known as "artificial atoms" because they provide the opportunity to control the energy of carrier states by adjusting the confinements in all three spatial dimensions. With QDs closely packed, the confined levels overlap to form minibands in QD superlattices. This extends the range of electronic and optical properties that can be provided by semiconductor materials. With the control of miniband energy level and bandwidth, QD superlattices have interesting possible applications in "third-generation" PV, especially for tandem solar cells. QDs have already been used successfully to improve the performance of devices such as lasers, light-emitting diodes, and photodetectors.

The basic principle behind the efficiency increases offered by QD intermediate-band solar cells is that the discrete states that result from the inclusion of the dots allow for absorption of sub-bandgap energies. The reason that this approach can exceed the efficiency of an ordinary dual-junction cell is that when the current is extracted, it is limited by the host bandgap and not the individual photon energies. In a dual-junction solar cell, the current must be "matched" between the two junctions. This means that the same amount of current must be passed through both junctions; therefore, the overall device efficiency is limited by the current-generating ability of the weaker of the two junctions. In addition, if a dual-junction or other multi-junction device is grown monolithically, with the junctions connected in series, then there must be tunnel junctions grown between the various active regions. Problems with lattice mismatch and the increased number of interfaces (and consequently, interfacial defects) are impediments to this approach. Although tremendous achievements have been made in developing multi-junction solar cells, this problem will be compounded with increasing the number of junctions. These problems with lattice mismatch and interfacial defects have plagued the development of multiple quantum well structures. The operation of the first prototype QD intermediate-band solar cell was presented by Marti et al. (2006). Theoretical results for the effect of dot size, interdot distance, and matrix material have been obtained by Jiang and Green (2006). These results clarify the required design features of silicon QD superlattices for proposed all-silicon tandem solar cells. Different aspects of QD solar cells were discussed in an excellent review by Nozik (2002).

7.3. Dye-sensitized solar cells

Dye-sensitized solar cells (DSSCs) have been extensively studied for their reasonable photoelectric conversion efficiency, simple assemble technology, and potential low cost. The sensitization of wide-bandgap semiconductors, such as ZnO, by organic dyes was investigated by several research groups (Gerischer and Tributsch, 1968; Hauffe et al., 1970) for photoelectrochemical (PEC) processes. A conversion efficiency of 1% in dye-sensitized ZnO photoelectrodes was achieved by Tsubomura et al. (1976). The first use of a dye-sensitized TiO_2 particle and thin film in a PEC configuration was reported by Deb et al. (1978). The PEC approach to solar energy conversion then shifted toward the use of narrow-bandgap semiconductors (e.g., Si, GaAs, CdSe) in conjunction with electrolytes, the analog of metal–semiconductor Schottky-barrier devices.

DSSCs based on liquid electrolytes have reached efficiencies as high as 10% under AM 1.5 (Nazeeruddin et al., 1993). However, the use of liquid electrolyte has created difficulties in sealing and the long-term photochemical stability of the device (Papageorgiou et al., 1997). To overcome these problems, researchers have attempted to replace the liquid electrolytes with solid or quasi-solid charge-transport materials (Nogueira et al., 2001). Compared with other types of charge-transport materials, the

gel electrolytes show higher ambient ionic conductivity (6–8 mS/cm) and better stability. Therefore, several types of gel electrolytes have already been used in quasi-solid-state DSSCs (Stathatos and Lianos, 2003; Wang et al., 2004). Organic–inorganic nanocomposites such as gel electrolytes like sol–gel silica can solidify liquid electrolytes, and higher overall energy conversion efficiencies have been achieved (Stathatos et al., 2004). However, the use of a liquid electrolyte and long-term stability remain as barriers to further technology development.

The field of DSSC research gained significant worldwide interest after Graetzel et al. reported the use of a Ru-based dye to achieve higher efficiency in a cell made of TiO_2 nanoparticles (O'Regan and Graetzel, 1991). They achieved a major improvement in solar energy conversion efficiency of 11% in a dye-sensitized TiO_2 (anatase) thin-film solar cell (Graetzel, 2001). This accomplishment was demonstrated in a PEC device consisting of a nanocrystalline and mesoporous TiO_2 (anatase) thin-film electrode sensitized by a stable Ru-terpyridine complex dye in non-aqueous solvent. Studies of low-temperature fabrication of TiO_2 on a flexible conductive film were investigated to realize a high-speed and low-cost manufacturing process of DSSC modules.

DSSCs exhibit energy conversion compatible to a-Si thin-film solar cells of about 10%, but can be produced at much lower cost (Ekins-Daukes et al., 2000; Green, 2004). Nanocrystals can increase the surface area of the cell more than 1000-fold, allowing it to absorb even more dye. Recent results in this field have been reviewed by several researchers (Arakawa and Hara, 2003; Stathatos et al., 2004; Deb, 2005; Gratzel, 2005; Li et al., 2006).

7.4. Organic solar cells

With a theoretical efficiency that is the same as conventional semiconductor devices and a cost structure derived from plastic processing, organic PV cells offer the long-term potential of achieving the goal of a PV technology that is economically viable for large-scale power generation. The first highly conductive polymer—chemically doped polyacetylene—was reported by Chiang et al. (1977). Organic molecules and semiconducting polymers are being increasingly used in optoelectronic devices. Some key advantages for organic PV are that organic small-molecule and polymer materials are inherently inexpensive; they can have very high optical absorption coefficients that permit the use of films with thicknesses of only several hundred nanometers; they are compatible with plastic substrates; and they can be fabricated using high-throughput, low-temperature approaches that employ one of a variety of well-established printing techniques in a roll-to-roll process. The ability to design and synthesize molecules and then integrate them into organic–organic and inorganic–organic composites provides a unique pathway in the design of materials for novel devices. A key issue faced by the organic electronics community in general is the stability of the organic materials. Device degradation pathways stem largely from changes in morphology, loss of interfacial adhesion, and interdiffusion of components, as opposed to strictly chemical decomposition. Thus, careful design and materials engineering can substantially improve device lifetimes.

Using a copper phthalocyanine layer as the donor and a perylene derivative as the acceptor, Tang (1986) first accomplished the structure of positive electrode/donor/acceptor/negative electrode. This device had a power conversion efficiency of about 1% under simulated solar illumination. As a result of the excitonic nature of the photoexcitations in organic solar cells, the operational mechanisms of organic PV are different from those of conventional PV. These differences are described in detail by Gregg (2005). One significant limitation of almost all organic compounds is their relatively narrow absorption spectra. Hence, it is not feasible to absorb the entire solar spectrum using a single donor–acceptor pair forming the organic PV cell. Furthermore, the open-circuit voltage produced by most organic hetero-junction cells is small—typically ranging between 0.4 and 0.8 V.

To improve the absorption of the solar radiation by organic solar cells, materials with a broad absorption band have to be designed and produced, or different narrow-band absorbers have to be stacked or mixed in multiple junctions (Peumans et al., 2003). When two (or more) donor materials with non-overlapping absorption spectra are used in a tandem (or multi-junction) solar cell, a broader range of the solar spectrum—the whole visible and part of the infrared range—can be covered.

Forrest (2005) showed that a combination of strategies has led to a power conversion efficiency of 5.7% for tandem cells based on small-molecular weight materials, suggesting that even higher efficiencies are possible. The status and future prospects of organic PV were discussed in excellent reviews by Peumans and Hadipour (Peumans et al., 2003; Hadipour et al., 2008).

7.5. Rectenna conversion

A revolutionary new approach suggested by Bailey in 1972 focuses on the wave nature of light. Bailey (1972) suggested that broadband rectifying antennas could be used for solar to direct-current (DC) conversion. These rectennas would not face the fundamental issue of a semiconductor's bandgap limiting conversion efficiency. Rectennas for solar conversion would have dimensions on the order of the wavelengths of solar radiation that falls mostly in the sub-micron range.

The primary advantage of the antenna approach to solar energy conversion is that conversion would not be bandgap limited, as it is in PV cells. In making this assertion, it is assumed that the process of rectifying high-frequency electromagnetic waves will not involve any such lossy quantum effects.

The idea of converting solar energy into useful d.c. electricity using antennas was first patented by J.C. Fletcher of

NASA and R.L. Bailey of the University of Florida, based on a project at NASA Goddard Center in the late 1960s (Fletcher and Bailey, 1973). The patent describes the concept as a device for converting electromagnetic wave energy into electric power and consisting of a number of relatively close-spaced electromagnetic wave absorber elements with tapered portions responsive to wide-band electromagnetic wave radiation.

Farber (1988) worked on the antenna-based energy conversion concept at the University of Florida's Solar Energy and Energy Conversion Laboratory. As a part of his work, he transmitted microwave radiation in the 0.2–3-GHz range using broadband metallic pyramidal antenna elements across the laboratory, where it was picked up by pyramidal dielectric antennas and rectified to DC power. This power was used to run a small motor as a proof of concept. Farber's work covered three frequency ranges: 0.2–3, 10, and 100 GHz. The bulk of his work was done at 10 GHz, where he characterized hollow dielectric pyramidal antennas to determine parameters such as optimum base size, length-over-base ratio, and array spacing. Some spot checks of those results were performed at 100 GHz. Farber also used a suitably modified carborundum paper in which the paper backing was scraped thin and metallic current collector wires randomly applied, to test under visible light. The grade of the paper was such that the SiC particles were about the right size as determined from his earlier experimentation. Some output was observed by testing, but it is not clear whether that was because of the antenna effect.

Lin et al. (1996) reported seeing a short-circuit current using a fabricated sub-nanostructure consisting of a parallel dipole array connected to a rectification arrangement. This is possibly the first and only experimental observation of resonance light absorption and rectification in the visible light range. Dipole antennas are linearly polarized antennas. Suh et al. (2000) obtained a maximum conversion efficiency of 60% using a circularly polarized truncated-corner square patch microstrip antenna at 5.8 GHz. Yoo and Chang (1992) also tested rectennas at 10 and 35 GHz with conversion efficiencies of 60% and 39%, respectively. The limitation in these tests was found to be with the diodes used for rectification.

Rectennas have been proposed for a wide range of applications, particularly wireless electrical power transmission and various radio-powered devices (Corkish et al., 2002). They have been demonstrated to have achieved very highly efficient conversion, exceeding 80%, to DC electricity from monochromatic microwave radiation (Brown, 1970) and have been theoretically predicted to be "capable of nearly 100% absorption of a perpendicularly incident planar beam" at a single frequency (Ott et al., 1981). The past, present, and future of rectenna conversion are reviewed by Goswami et al. (2004).

Two fundamental physical limitations—skin effect resistance and very low voltage per antenna element—were identified for the rectenna system. The issues associated with the antenna are polarization, bandwidth, efficiency, and impedance matching. These issues are well discussed by Sarehraz et al. (2005), and it was shown that a linear array of high-gain antenna elements feeding each diode has a much better possibility of success. The antenna-coupled metal–insulator–metal (MIM) detector can operate at ambient temperature and used as a detector and harmonic mixer up to 150 THz. In a MIM tunnel diode, the electrons flow between the metal electrodes via an ultra-thin insulator layer. This concept has been exploited for reliable rectification in the high-frequency (NGHz) regime for the desired application. The MIM diode rectifies electromagnetic radiation induced by the antenna through two dominant phenomena: thermionic emission and quantum mechanical tunnelling. Effects of dielectric thickness and contact area on current–voltage characteristics of thin-film MIM diodes were studied by Krishnan et al. (in press-a). The authors of this work concluded that fabricated MIM diodes will eventually be used as a rectenna element for infrared detection.

The design, fabrication, and characterization aspect of a thin-film MIM diode for infrared detection were studied by Krishnan et al. (in press-b). In this work, the detector circuit demonstrated excellent output voltage and sensitivity at a power of 8 and −37 dBm, respectively. When the antenna and the detector were combined to measure its rectification effects, a significant level of DC output was measured across the system. The recent developments in nanotechnology and manufacturing led to the re-examination of the rectenna concept for solar energy collection.

8. Conclusions

The present PV market is growing at the very high rate of 35–40% per year, and world PV production was 10.66 GW in 2009. More than 80% of the world PV industry is based on c-Si and pc-Si wafer technologies. Single-junction c-Si and GaAs solar cells are approaching their upper limits in terms of the theoretical maximum efficiency. Remarkable efficiency results have been achieved in the field of thin-film solar cells: 19–20% CIGS and 16–17% CdTe and Si polycrystalline thin-film solar cells. III–V multi-junction solar cells have obtained about 40% efficiency. The recent developments in nanotechnology and manufacturing led to the re-examination of the rectenna concept for solar energy collection. Further R&D will be directed toward increasing the efficiency of thin-film CIGS, CdTe, and Si and multi-junction III–V cells and nano-PV devices. However, for most of the leading technologies, the efficiency is already adequate, and emphasis should be on developing cost-effective manufacturing technologies that can significantly lower the module production cost below US$ 1.5/W_p for c-Si.

References

Abken, A.E., Bartelt, O.J., 2002. Sputtered Mo/Sb_2Te_3 and Ni/Sb_2Te_3 layers as back contacts for CdTe/CdS solar cells. Thin Solid Films 403–404, 216–222.

Amin, N., Isaka, T., Yamada, A., Konagai, M., 1999. High efficient 1 μm thick CdTe solar cells with textured TCOs. In: Technical Digest of the 11th International Photovoltaic Science and Engineering Conference, Sapporo, Japan, pp. 837–838.

Andreev, V.M., 1994. High efficiency (24.6%, AMO) LPE grown AlGaAs/GaAs concentrator solar cells and modules. In: Proceedings of the First WCPEC, Hawaii, USA, pp. 2096–2099.

Arakawa, H., Hara, K., 2003. In: Schanze, K., Rammurthy, V. (Eds.), . In: Current Status of Dye-sensitized Solar Cells, Semiconductor Photochemistry, and Photophysics, vol. 10. Marcel Dekker, New York, pp. 123–171.

Aramoto, T., Kumazawa, S., Higuchi, H., Arita, T., Shibutani, S., Nishio, T., Nakajima, J., Murozono, M., 1997. 16.0% efficient thin-film CdS/CdTe solar cells. Japanese Journal of Applied Physics, Part 1: Regular Papers and Short Notes and Review Papers 36 (10), 6304–6305.

Araujo, G.L., Marti, A., 1994. Absolute limiting efficiencies for photovoltaic energy conversion. Solar Energy Materials and Solar Cells 33, 213–240.

Ashenford, D.E., Dweydare, A.W., Sands, D., Scott, C.G., Yousaf, M., Aperathitis, E., Hatzopoulos, Z., Panagotatos, P., 1995. Investigation of p–i–n solar cell efficiency enhancement by use of MQW structures in the i-region. Journal of Crystal Growth 159, 920–924.

Bailey, R.L., 1972. A proposed new concept for a solar energy convertor. Journal of Engineering for Power 94, 73–77.

Barnham, K.W.J., Abbott, P., Ballard, I., Bushnell, D.B., Connolly, J.P., Ekins-Daukes, N.J., Mazzer, M., Nelson, J., Rohr, C., Tibbits, T.N., Airey, R., Hill, G., Roberts, J.S., 2003. Recent results on quantum well solar cells. In: Proc. of the 3rd World Conference on Photovoltaic Energy Conversion, VA, pp. 606–611.

Basore, P.A., 2004. Simplified processing and improved efficiency of crystalline silicon on glass modules. In: 19th European Photovoltaic Solar Energy Conference, Paris, June, pp. 455–458.

Bätzner, D.L., Romeo, A., Zogg, H., Wendt, R., Tiwari, A.N., 2001. Development of efficient and stable back contacts on CdTe/CdS solar cells. Thin Solid Films 387 (1–2), 151–154.

Bätzner, D.L., Romeo, A., Terheggen, M., Döbeli, M., Zogg, H., Tiwari, A.N., 2004. Stability aspects in CdTe–CdS solar cells. Thin Solid Films 451–452, 536–543.

Bhattacharya, R.N., Ramanathan, K., 2004. $Cu(In,Ga)Se_2$ thin film solar cells with buffer layer alternative to CdS. Solar Energy 77, 679–683.

Britt, J., Ferekides, C., 1993. Thin film CdS/CdTe solar cell with 15.8% efficiency. Applied Physics Letters 62, 2851–2852.

Brown, W.C., 1970. The receiving antenna and microwave power rectification. Journal of Microwave Power 5, 279.

Carlson, D., Wronski, C., 1976. Amorphous silicon solar cell. Applied Physics Letters 28, 671–673.

Chaisitsak, S., Yamada, A., Konagai, M., 2001. In: The Proceedings of the Materials Research Society Spring Meeting, San Francisco, p. 668.

Chiang, C.K., Fincher Jr., C.R., Park, Y.W., Heeger, A.J., Shirakawa, H., Louis, E.J., Gau, S.C., MacDiarmid, A.G., 1977. Electrical conductivity in doped polyacetylene. Physical Review Letters 39, 1098–1101.

Compaan, A.D., 2004. The status of and challenges in CdTe thin-film solar-cell technology. MRS Symposium Proceedings 808, 545–555.

Corkish, R., Green, M.A., Puzzer, T., 2002. Solar energy collection by antennas. Solar Energy 73, 395.

Cusano, D.A., 1963. CdTe solar cells and photovoltaic heterojunctions in II–VI compounds. Solid State Electronics 6 (3), 217–232.

De Vos, A., Desoete, B., 1998. On the ideal performance of solar cells with larger-than-unity quantum efficiency. Solar Energy Materials and Solar Cells 51, 413–424.

De Vos, A., Pauwels, H., 1981. On the thermodynamic limit of photovoltaic energy conversion. Journal of Applied Physics 25, 119–225.

Deb, S.K., 2005. Dye-sensitized TiO_2 thin-film solar cell research at the National Renewable Energy Laboratory (NREL). Solar Energy Materials & Solar Cells 88, 1–10.

Deb, S.K., Chen, S., Witzke, H., 1978. US Patents 4117510, 4080488, 4118246, and 4118247.

Deng, X., Schiff, E.A., 2003. Amorphous silicon–based solar cells. In: Luque, A., Hegedus, S. (Eds.), Handbook of Photovoltaic Science and Engineering. John Wiley & Sons.

Diefenbach, K.H., 2005. Wiped away. Photon International, 48–67.

Eberspacher, C., Fredric, C., Pauls, K., Serra, J., 2001. Thin-film CIS alloy PV materials fabricated using non-vacuum, particles-based techniques. Thin Solid Films 387, 18–22.

Ebil, O., Aparicio, R., Birkmire, R., 2004. In-situ AIC of Si thin films on glass above the eutectic point using HWCVD. In: MRS Symp. Proc., vol. 808, pp. 321–326.

Ekins-Daukes, N., Bushnell, D., Zhang, J., Barnham, K., Mazzer, M., 2000. Strain-balanced materials for high-efficiency solar cells. In: Proc.28th IEEE PV Specialists Conference, USA, pp. 1273–1276.

Ellingson, R.J., Beard, M.C., Johnson, J.C., Yu, P., Micic, O.I., Nozik, A.J., 2005. Highly efficient multiple exciton generation in colloidal PbSe and PbS quantum dots. Nano Letters 5, 865–871.

Farber, E.A., 1988. Antenna Solar Energy to Electricity Conversion. Report to the Airforce, AF C F08635-83-C-0136, Task 85-6.

Feng, Z.C., Chou, H.C., Rohatgi, A., Lim, G.K., Wee, A.T.S., Tan, K.L., 1996. Correlations between $CdTe/CdS/SnO_2$/glass solar cell performance and the interface/surface properties. Journal of Applied Physics 79 (4), 2151–2153.

Fletcher, J.C., Bailey, R.L., 1973. Electromagnetic wave energy converter. US Pat. No. 3760257.

Forrest, S.R., 2005. The limits to organic photovoltaic cell efficiency. MRS Bulletin 30 (1), 28–32.

Fthenakis, V., Zweibel, K., 2003. CdTe PV: Real and Perceived EHS Risks. Prepared for the NCPV and Solar Program Review Meeting, March 25, 2003.

Fthenakis, V., Morris, S., Moskowitz, P., Morgan, D., 1999. Toxicity of cadmium telluride, copper indium diselenide, and copper gallium diselenide. Progress in Photovoltaics 7, 489–497.

Gabor, A.M., Tuttle, J.R., Albin, D.S., Contreras, M.A., Hermann, A.M., Noufi, R., 1994. High-efficiency $CuIn_xGa_{1-x}Se_2$ solar cells made from $(In_x,Ga_{1-x})_2Se_3$ precursor films. Applied Physics Letters 65, 198–200.

Gerischer, H., Tributsch, H., 1968. Elecrochemische Untersuchungen zur spectraleu sensibilisierung von ZnO-Einkristalien. Berichte der Bunsengesellschaft für Physikalische Chemie 72, 437–445.

Goetzberger, A., Hebling, C., Schock, H.W., 2003. Photovoltaic materials, history, status and outlook. Materials Science and Engineering, R 40, 1–46.

Goswami, D.Y., Vijayaraghavan, S., Lu, S., Tamm, G., 2004. New and emerging developments in solar energy. Solar Energy 76, 33–43.

Graetzel, M., 2001. Photoelectrochemical Cells. Nature 414, 338–344.

Granqvist, C.G., 2003. Solar energy materials. Advance Materials 15, 1789–1803.

Gratzel, M., 2005. Solar energy conversion by dye-sensitized photovoltaic cells. Inorganic Chemistry 44 (20), 6841–6851.

Green, M.A., 2000a. Status of crystalline photovoltaic technology. In: World Renewable Energy Congress VI, pp. 2630–2635.

Green, M.A., 2000b. Prospects for photovoltaic efficiency enhancement using low dimensional structures. Nanotechnology 11, 402–405.

Green, M.A., 2002. Third generation photovoltaics: solar cells for 2020 and beyond. Physica E 14 (1–2), 65–70.

Green, M.A., 2004. Recent developments in photovoltaics. Solar Energy 76, 3–8.

Green, M.A., Zhao, J., Wang, A., Wenhan, S.R., 2001. Progress and outlook for high efficiency crystalline silicon solar cells. Solar Energy Materials and Solar Cells 65, 9–16.

Gregg, B.A., 2005. The photoconversion mechanism of exitonic solar cells. MRS Bulletin 30 (1), 20–22.

Guha, S., 1992. Amorphous silicon alloy technology for photovoltaics. In: Proceedings of the 6th International Photovoltaic Science and Engineering Conference, New Delhi, India, pp. 55–60.

Guha, S., 2004. Thin film silicon solar cells grown near the edge of amorphous to microcrystalline transition. Solar Energy 77, 887–892.

Guha, S., Narsimhan, K.L., Pietruszko, S.M., 1981. On light-induced effect in amorphous hydrogenated silicon. Journal of Applied Physics 52, 859–860.

Guha, S., Yang, J., Nath, P., Hack, M., 1986. Enhancement of open circuit voltage in high efficiency amorphous silicon alloy solar cells. Applied Physics Letters 49, 218–219.

Gupta, A., Compaan, A.D., 2003. 14% CdS/CdTe thin film cells with ZnO:Al TCQ. In: Materials Research Society Symposium – Proceedings, vol. 763, pp. 161–166.

Hadipour, A., de Boer, B., Blom, P.W.M., 2008. Organic tandem and multi-junction solar cells. Advanced Functional Materials 18, 169–181.

Hamakawa, Y., 1994. Recent advances of thin film solar cells and their technologies. In: Proceedings of the First World Conference on Photovoltaic Energy Conversion, Hawaii, USA, pp. 34–41.

Hanna, M.C., Nozik, A.J., 2006. Solar conversion efficiency of photovoltaic and photoelectrolysis cells with carrier multiplication absorbers. Journal of Applied Physics 100, 074510-1–074510-8.

Hartley, A., Irvine, S.J.C., Halliday, D.P., Potter, M.D.G., 2001. The influence of CdTe growth ambient on MOCVD grown CdS/CdTe photovoltaic cells. Thin Solid Films 387 (1–2), 89–91.

Hauffe, K., Danzmann, H.J., Pusch, H., Range, J., Volz, H., 1970. New experiments on the sensitization of zinc oxide by means of the electrochemical cell technique. Journal of the Electrochemical Society 117, 993–999.

Hedström, J., Ohlsen, H., Bodegard, M., Kylner, A., Stolt, L., Hariskos, D., Ruckh, M., Schock, H.W., 1993. ZnO/CdS/Cu(In,Ga)Se_2 thin film solar cells with improved performance. In: The Proceedings of the 23rd IEEE Photovoltaic Specialists Conference, New York, pp. 364–371.

Inomota, V., Fukui, K., Shirasawa, K., 1996. Surface texturing of large area multicrystalline silicon solar cells using reactive ion etching method. In: Technical Digest, 9th International Photovoltaic Science and Engineering Conference, Miyazaki, Japan, pp. 109–110.

Jiang, C.W., Green, M.A., 2006. Silicon quantum dot superlattices: modeling of energy bands, densities of states, and mobilities for silicon tandem solar cell applications. Journal of Applied Physics 99, 114902.

Kaelin, M., Rudmann, D., Tiwari, A.N., 2004. Low cost processing of CIGS thin film solar cells. Solar Energy 77, 749–756.

Karg, F.H., 2001. Development and manufacturing of CIS thin film solar modules. Solar Energy Materials and Solar Cells 66, 645.

Kazmerski, L., 2006. Solar photovoltaics R&D: at the tipping point: a 2005 technology overview. Journal of Electron Spectroscopy and related Phenomena 150 (2–3), 105–135.

Kazmerski, L.L., White, F.R., Morgan, G.K., 1976. Thin-film $CuInSe_2$/CdS heterojunction solar cells. Applied Physics Letters 29, 268–270.

Kessler, F., Rudmann, D., 2004. Technological aspects of flexible CIGS solar cells and modules. Solar Energy 77, 685–695.

Klein, S., Repmann, T., Brammer, T., 2004. Microcrystalline silicon films and solar cells deposited by PECVD and HWCVD. Solar Energy 77, 893–908.

Kodolinski, S., Werner, J.H., Wittchen, T., Queisser, H.J., 1993. Quantum efficiencies exceeding unity due to impact ionization in silicon solar cells. Applied Physics Letters 63 (17), 2405–2407.

Krishnan, S., Stefanakos, E., Bhansali, S., 2008a. Effects of dielectric thickness and contact area on current–voltage characteristics of thin film metal–insulator–metal diodes. Thin Solid Films 516 (8), 2244–2250.

Krishnan, S., La Rosa, H., Bhansali, S., Buckle, K., Stefanakos, E., 2008b. Design and development of batch fabricatable metal–insulator–metal diode and microstrip slot antenna as rectenna elements. Sensors and Actuators 142 (1), 40–47.

Kushiya, K., 2004. Development of Cu(InGa)Se_2-based thin-film PV modules with a Zn(O,S,OH)$_x$ buffer layer. Solar Energy 77, 717–724.

Kushiya, K., Ohshita, M., Hara, I., Tanaka, Y., Sang, B., Nagoya, Y., Tachiyuki, M., Yamase, O., 2003. Yield issues on the fabrication of 30 cm × 30 cm-sized Cu(In,Ga)Se_2-based thin-film modules. Solar Energy Materials and Solar Cells 75 (1–2), 171–178.

Lebrun, J., 1966. Réalisation et propriétés des photopiles solaires en couches minces de tellurure de cuivre et tellurure de cadmium. Revue de Physique Appliquee 1 (3), 204–210.

Lechner, P., Schade, H., 2002. Photovoltaic thin-film technology based on hydrogenated amorphous silicon. Progress in Photovoltaics: Research and Applications 10, 85–97.

Li, B., Wang, L., Kang, B., Wang, P., Qiu, Y., 2006. Review of recent progress in solid-state dye-sensitized solar cells. Solar Energy Materials and Solar Cells 90 (5), 549–573.

Lin, G.H., Abdu, R., Bockris, J.O., 1996. Investigation of resonance light absorption and rectification by subnanostructures. Journal of Applied Physics 80 (1), 565–568.

Luque, A., Marti, A., 1997. Increasing the efficiency of ideal solar cells by photon induced transitions at intermediate levels. Physical Review Letters 78 (14), 5014–5017.

Marsillae, S., Paulson, P.D., Haimbodi, M.W., Birkmire, R.W., Shafarman, W.N., 2002. High efficiency solar cells based on Cu(In,Al)Se_2 thin films. Applied Physics Letters 81, 1350–1355.

Marti, A., Araujo, G.L., 1996. Limiting efficiencies for photovoltaic energy conversion in multigap systems. Solar Energy Materials and Solar Cells 43, 203–222.

Marti, A., Lopez, N., Antolın, E., Canovas, E., Stanley, C., Farmer, C., Cuadra, L., Luque, A., 2006. Novel semiconductor solar cell structures: the quantum dot intermediate band solar cell. Thin Solid Films 511–512, 638–644.

Mathew, X., Thompson, G.W., Singhc, V.P., McClured, J.C., Velumania, S., Mathews, N.R., Sebastian, P.J., 2003. Development of CdTe thin films on flexible substrates – a review. Solar Energy Materials & Solar Cells 76, 293–303.

Matsuda, A., Yamaoka, T., Wolf, S., Koyama, M., Imanishi, Y., Kataoka, H., Matsumara, H., Tanaka, K., 1986. Preparation of highly photosensitive hydrogenated amorphous Si–C alloys from a glow-discharge plasma. Journal of Applied Physics 60, 4025–4027.

Maycock, P.D., 2010. PV News, V.29, N5.

Mazzer, M., Barnham, K.W.J., Ballard, I.M., Bessiere, A., Ioannides, A., Johnson, D.C., Lynch, M.C., Tibbits, T.N.D., Roberts, J.C., Hill, G., Calder, C., 2006. Progress in quantum well solar cells. Thin Solid Films 511–512, 76–83.

McCandless, B.E., Dobson, K.D., 2004. Processing options for CdTe thin film solar cells. Solar Energy 77, 839–856.

McCandless, B.E., Sites, J.R., 2003. Cadmium telluride solar cells. In: Luque, A., Hegedus, S. (Eds.), Handbook of Photovoltaic Science and Engineering. John Wiley & Sons, Ltd.

Mendoza-Peŕez, R., Santana-Rodŕıguez, G., Sastre-Hernández, J., Morales-Acevedo, A., Arias-Carbajal, A., Vigil-Galan, O., Alonso, J.C., Contreras-Puente, G., 2005. Effects of thiourea concentration on CdS thin films grown by chemical bath deposition for CdTe solar cells. Thin Solid Films 480–481, 173–176.

Miyake, M., Murase, K., Hirato, T., Awakura, Y., 2004. Hall effect measurements on CdTe layers electrodeposited from acidic aqueous electrolyte. Journal of Electroanalytical Chemistry 562 (2), 247–253.

Muller, J., Rech, B., Springer, J., Vanecek, M., 2004. TCO and light trapping in silicon thin film solar cells. Solar Energy 77, 917–930.

Murphy, J.E., Beard, M.C., Norman, A.G., Ahrenkiel, S.P., Johnson, J.C., Yu, P., Micic, O.I., Ellingson, R.J., Nozik, A.J., 2006. PbTe colloidal nanocrystals: synthesis, characterization, and multiple exciton generation. Journal of the American Chemical Society 128, 3241–3247.

Nakada, T., Mizutani, M., 2002. 18% Efficiency Cd-free Cu(In,Ga)Se_2 thin-film solar cells fabricated using chemical bath deposition (CBD)-ZnS buffer layers. Japanese Journal of Applied Physics 41, L165–L167.

Nakada, T., Hirabayashi, Y., Tokado, T., Ohmori, D., Mise, T., 2004. Novel device structure for Cu(In,Ga)Se_2 thin film solar cells using transparent conducting oxide back and front contacts. Solar Energy 77, 739–747.

Nazeeruddin, M.K., Kay, A., Rodicio, I., Humphry, R., Muller, E., Gratzel, M., 1993. Conversion of light to electricity by cis-X_2 bis (2,2′-bipyridyl-4,4′-dicarboxylate) ruthenium (II) charge-transfer sensitizers ($X = Cl^-$, Br^-, I^-, CN^- and SCN^-) on nanocrystalline titanium dioxide electrodes. Journal of American Chemical Society 115, 6382–6391.

Nogueira, A.F., Marco, A., DePaoli, M.A., Montanari, I., Monkhouse, R., Nelson, J., Durrant, J.R., 2001. Electron transfer dynamics in dye sensitized nanocrystalline solar cells using a polymer electrolyte. Journal of Physical Chemistry B 105, 7517–7524.

Nozik, A.J., 2002. Quantum dot solar cells. Physica E 14 (1–2), 115–120.

Ohtake, Y., Kushiya, K., Ichikawa, M., Yamada, A., Konagai, M., 1995. Polycrystalline Cu(InGa)Se_2 thin-film solar cells with ZnSe buffer layers. Japanese Journal of Applied Physics 34, 5949–5955.

O'Regan, B., Graetzel, M., 1991. A low-cost, high efficiency solar cell based on dye-sensitized colloidal TiO_2 films. Nature 353, 737–740.

Ott, J.H., Rice, J.S., Thorn, D.C., 1981. A theoretical study of microwave beam absorption by a rectenna. NASA Lyndon B. Johnson Space Center NAS9-16055, 14 January.

Palm, J., Probst, V., Karg, F.H., 2004. Second generation CIS solar modules. Solar Energy 77, 757–765.

Papageorgiou, N., Maier, W., Grätzel, M., 1997. An iodine/triiodide reduction electrocatalyst for aqueous and organic media. Journal of the Electrochemical Society 144, 876–884.

Pauwels, H., de Vos, A., 1981. Determination of the maximum efficiency solar cell structure. Solid State Electronics 24, 835–843.

Peumans, P., Yakimov, A., Forrest, S.R., 2003. Small molecular weight organic thin-film photodetectors and solar cells. Journal of Applied Physics 93, 3693–3723.

Ramanathan, K., Contreras, M.A., Perkins, C.L., Asher, S., Hasoon, F., Keane, J., Young, D., Romero, M., Metzger, W., Noufi, R., Ward, J., Duda, A., 2003. Properties of 19.2% efficiency ZnO/CdS/CuInGaSe_2 thin film solar cells. Progress in Photovoltaics: Research and Applications 11, 225–230.

Razykov, T.M., 1991. Chemical molecular beam deposition of II–VI binary and ternary compound films in gas flow. Applied Surface Science 48 (49), 89–92.

Razykov, T.M., 1996. A new conception on the passivation of the grain boundaries of polycrystalline thin film solar cells. In: Abstracts of the International Conf. EuroSun' 96. Freiburg, Germany, pp. V-91–V-92.

Razykov, T.M., Rech, B., Tiwari, A.N. (Eds.), 2004. Special issue on thin Film PV. Solar Energy, N6.

Razykov, T.M., Contreras-Puente, G., Chornokur, G., Dybjec, M., Emirov, Y., Ergashev, B., Ferekides, C., Goswami, Y., Hubbimov, A., Ikramov, B., Kouchkarov, K., Mathew, X., Morel, D., Ostapenko, S., Sanchez-Meza, S., Stefanakos, E., Vigil-Galan, O., Vorobiev, Y., Zhao, H., 2007. Effect of $CdCl_2$ treatment on structure and photoluminescence of CdTe films with different compositions fabricated by CMBD. Technical Digest of the International PVSEC-17, Fukuoka, Japan, 5P-P3-43, pp. 855–856.

Razykov, T.M., Contreras-Puente, G., Chornokur, G.C., Dybjec, M., Emirov, Yu., Ergashev, B., Ferekides, C.S., Hubbimov, A., Ikramov, B., Kouchkarov, K.M., Mathew, X., Morel, D., Ostapenko, S., Sanchez-Meza, E., Stefanakos, E., Upadhyaya, H.M., Vigil-Galan, O., Vorobiev, Yu.V., 2009. Structural, photoluminescent and electrical properties of CdTe films with different compositions fabricated by CMBD. Solar Energy 83, 90–93.

Rech, B., Wagner, H., 1999. Potential of amorphous silicon for solar cells. Applied Physics A 69, 155–167.

Repins, I., Contreras, M.A., Egaas, B., DeHart, C., Scharf, J., Perkins, C.L., To, B., Noufi, R., 2008. 19.9%-efficient ZnO/CdS/CuInGaSe_2 solar cell with 81.2% fill factor. Progress in Photovoltaics: Research and Applications 16, 235–239.

Romeo, N., Bosio, A., Tedeschi, R., Romeo, A., Canevari, V., 1999. A highly efficient and stable CdTe/CdS thin film solar cell. Solar Energy Materials and Solar Cells 58 (2), 209–218.

Romeo, N., Bosio, A., Tedeschi, R., Canevari, V., 2000. Growth of polycrystalline CdS and CdTe thin layers for high efficiency thin film solar cells. Materials Chemistry and Physics 66, 201–206.

Ross, R.T., Nozik, A.J., 1982. Efficiency of hot-carrier solar energy converters. Journal of Applied Physics 53 (5), 3813–3818.

Sarehraz, M., Buckle, K., Weller, T., Stefanakos, E., Bhansal, S., Goswami, Y., Krishnan, S., 2005. Rectenna developments for solar energy collection. In: 31st IEEE Photovoltaic Specialists Conference, Orlando, USA, pp. 78–81.

Schaller, R.D., Klimov, V.I., 2004. High efficiency carrier multiplication in PbSe nanocrystals: implications for solar energy conversion. Physical Review Letters 92 (18), 186601-1–186601-4.

Schaller, R.D., Klimov, V.I., 2006. Non-poissonian exciton populations in semiconductor nanocrystals via carrier multiplication. Physical Review Letters 96, 097402-1–097402-4.

Schaller, R.D., Petruska, M.A., Klimov, V.I., 2005. Effect of electronic structure on carrier multiplication efficiency: comparative study of PbSe and CdSe nanocrystals. Applied Physics Letters 87 (25), 253102–253103.

Schaller, R.D., Sykora, M., Pietryga, J.M., Klimov, V.I., 2006. Seven excitons at a cost of one: redefining the limits for conversion efficiency of photons into charge carriers. Nano Letters 6 (3), 424–429.

Schock, H.W., Pfisterer, F., 2001. Thin-film solar cells: past, present and future. Renewable Energy World (March–April), 75–87.

Shah, A.V., Schade, H., Vanecek, M., Meier, J., Vallat-Sauvain, E., Wyrsch, N., Kroll, U., Droz, C., Bailat, J., 2004. Thin-film silicon solar cell technology. Progress in Photovoltaics: Research and Applications 12, 113–142.

Shockley, W., Queisser, H.J., 1961. Detailed balance limit of efficiency of *p–n* junction solar cells. Journal of Applied Physics 32 (3), 510–519.

Sopori, B., 2003. Thin film Si solar cells. In: Luque, A., Hegedus, S. (Eds.), Handbook of Photovoltaic Science and Engineering. John Wiley & Sons, Ltd.

Spiering, S., Hariskos, D., Powalla, M., Naghavi, N., Lincot, D., 2003. CD-free Cu(In,Ga)Se_2 thin-film solar modules with In_2S_3 buffer layer by ALCVD. Thin Solid Films 431–432, 359–363.

Staebler, D.L., Wronski, C.R., 1977. Reversible conductivity changes in discharge-produced amorphous Si. Applied Physics Letters 31, 292–294.

Stathatos, E., Lianos, P., 2003. A quasi-solid-state dye-sensitized solar cell based on a sol–gel nanocomposite electrolyte containing ionic liquid. Chemistry of Materials 15, 1825–1829.

Stathatos, E., Lianos, P., Jovanovskib, V., Orel, B., 2004. Dye-sensitized photoelectrochemical solar cells based on nanocomposite organic–inorganic materials. Journal of Photochemistry and Photobiology A: Chemistry 169, 57–61.

Suh, Y.-H., Wang, C., Chang, K., 2000. Circularly polarized truncated-corner square patch microstrip rectenna for wireless power transmission. Electronics Letters 36 (7), 600–602.

Sundaram, V.S., Fraas, L.M., Gruenbaum, P.E., Avery, J.E., Maloesay, E., Kuryla, M.S., 1992. High efficiency tandem GaAs/GaSb concentrator solar cells. In: Proceedings of the 6th International Photovoltaic Science and Engineering Conference, New Delhi, India, pp. 395–400.

Tang, C.V., 1986. Two-layer organic photovoltaic cell. Applied Physics Letters 48 (2), 183–185.

Tobias, I., Luque, A., 2002. Ideal efficiency of monolithic, series-connected multijunction solar cells. Progress in Photovoltaics: Research and Applications 10 (5), 323–329.

Tsubomura, H., Matsumara, M., Nomura, Y., Amamiya, T., 1976. Dye sensitised zinc oxide: aqueous electrolyte: platinum photocell. Nature 261, 402–403.

Upadhyaya, H.M., Razykov, T.M., Tiwari, A.N., 2007. Thin film PV technology. In: Kreith, F., Goswami, D.Y. (Eds.), Handbook of Energy Conservation and Renewable Energy. CRC Press, NY, USA.

Vamsi Krishna, K., Dutta, V., 2004. Effect of in situ $CdCl_2$ treatment on spray deposited CdTe/CdS heterostructure. Journal of Applied Physics 96 (7), 3962–3971.

Vetterl, O., Finger, F., Carius, R., Hapke, P., Houben, L., Kluth, O., Lambertz, A., Mück, A., Rech, B., Wagner, H., 2000. Intrinsic microcrystalline silicon: a new material for photovoltaics. Soar Energy Materials and Solar Cells 62, 97–108.

von Roedern, B., 2003. Status of amorphous and crystalline thin-film silicon solar cell activities. NCPV and Solar Program Review Meeting 5, 552–555.

von Roedern, B., 2010. Data taken from websites.

von Roedern, B., Zweibel, K., Ullal, H.S., 2005. The role of polycrystalline thin-film PV technologies for achieving mid-term market-competitive PV modules. In: Proc. of the IEEE PVSC-31, Orlando, USA, pp. 1635–1638.

Wagner, S., Shay, J., Migliorato, P., Kasper, H., 1974. $CuInSe_2/CdS$ heterojunction photovoltaic detectors. Applied Physics Letters 25, 434.

Wang, P., Zakeeruddin, S.M., Grätzel, M., 2004. Solidifying liquid electrolytes with fluorine polymer and silicananoparticles for quasi-solid dye-sensitized solar cells. Journal of Fluorine Chemistry 125, 1241–1245.

Wang, Z.A., Zhu, H.B., Zhang, D.W., Shi, J.H., Li, X.D., Cheng, W.J., Sun, Z., Huang, S.M., 2009. Stability of transparent conducting oxide films deposited by sputtering for solar cells applications. In: Conference Record of the IEEE Photovoltaic Specialists Conference, Art. No. 5411587, pp. 000676–000679.

Wettling, W., 1995. High efficiency silicon solar cells: state of the art and trends. Solar Energy Materials and Solar Cells 38, 487–500.

Woggan, U., 1997. Optical Properties of Semiconductor Quantum Dots. Springer, Berlin.

Wu, X., Keane, J.C., DeHart, C., Albin, D.S., Duda, A., Gessert, T.A., Asher, S., Levi, D.H., Scheldon, P., 2001. 16.5% efficient CdS/CdTe polycrystalline thin film solar cell. In: Proc. of the 17th European Photovoltaic Solar Energy Conference, Munich, Germany, pp. 995–999.

Yamaguchi, M., Takamoto, T., Arak, K., Ekins-Daukes, N., 2005. Multijunction III–V solar cells: current status and future potential. Solar Energy 79 (1), 78–85.

Yamaguchi, Masafumi, Nishimura, Ken-Ichi, Sasaki, Takuo, Suzuki, Hidetoshi, Arafune, Kouji, Kojima, Nobuaki, Ohsita, Yoshio, Okada, Yoshitaka, Yamamoto, Akio, Takamoto, Tatsuya, Araki, Kenji, 2008. Novel materials for high-efficiency III–V multi-junction solar cells. Solar Energy 82, 173–180.

Yamamoto, K., Yoshimi, M., Tawada, Y., Okamoto, Y., Nakajima, A., 1999. Cost effective and high performance thin film Si solar cells towards the 21century. Technical Digest. The International PVSEC-11, Sapporo, Japan, pp. 225–228.

Yamamoto, K., Nakajima, A., Yoshimi, M., Sawada, T., Fukuda, S., Suezaki, T., Ichikawa, M., Koi, Y., Goto, M., Meguro, T., Matsuda, T., Kondo, M., Sasaki, T., Tawada, Y., 2004. A high efficiency thin film silicon solar cell and module. Solar Energy 77, 939–949.

Yoo, T.-W., Chang, K., 1992. Theoretical and experimental development of 10 and 35 GHz rectennas. IEEE Transactions on Microwave Theory and Techniques 40 (6), 1259–1266.

Zhao, J., Wang, A., Green, M.A., 1998. 19.8% efficient "honeycomb" textured multicrystalline and 24.4% monocrystalline silicon solar cells. Applied Physics Letters 73, 1991–1993.

Zhao, J., Wang, A., Green, M.A., 2001. High efficiency PERL and PERT silicon solar cells on FZ and MCZ Substrates. Solar Energy Materials and Solar Cells 65, 429–435.

Zolper, J.C., Narayanan, S., Wenham, S.R., Green, M.A., 1989. 16.7% efficiency, laser textured, buried contact polycrystalline silicon solar cells. Applied Physics Letters 55, 2363–2365.

Zweibel, K., 2005. The Terawatt challenge for thin film PV. In: Poortmans, J., Archipov, V. (Eds.), Thin Film Solar Cells: Fabrication, Characterization and Application. John Wiley, pp. 18–22.